

Host response during unresolved urinary tract infection alters mammary tissue homeostasis through collagen deposition and TIMP1

Authors: Samantha Henry^{1,2#}, Steven Macauley Lewis^{1,2#}, Samantha Leeanne Cyrill^{1#}, Mackenzie Kate Callaway¹, Deeptiman Chatterjee¹, Amritha Varshini Hanasoge Somasundara^{1,3}, Gina Jones^{1,4}, Xue-Yan He⁵, Giuseppina Caligiuri¹, Michael Francis Ciccone¹, Isabella Andrea Diaz¹, Amelia Biswas^{1,6}, Evelyn Hernandez¹, Taehoon Ha¹, John Erby Wilkinson⁷, Mikala Egeblad⁸, David Arthur Tuveson¹, Camila Oresco dos Santos^{1*}

Affiliations: ¹Cold Spring Harbor Laboratory; Cold Spring Harbor, NY, USA. ²Stony Brook University, Graduate Program in Genetics; Stony Brook, NY, USA. ³CSHL School of Biological Sciences; Cold Spring Harbor, NY, USA. ⁴CSHL Undergraduate Research Program; Cold Spring Harbor, NY, USA. ⁵Department of Cell Biology and Physiology. School of Medicine in St. Louis. Washington University, St. Louis., MO, USA. ⁶SUNY Downstate Health Sciences University, Neural and Behavior Science; Brooklyn, NY, USA. ⁷Department of Comparative Medicine, University of Washington; Seattle, WA, USA. ⁸Department of Cell Biology. Department of Oncology. School of Medicine. Johns Hopkins University. Baltimore, MD, USA.

these authors contributed equality

*corresponding author: dossanto@cshl.edu

Abstract: Exposure to pathogens throughout a lifetime influences immunity and organ function. Here, we explored how the systemic host-response to bacterial urinary tract infection (UTI) induces tissue-specific alterations to the mammary gland. Utilizing a combination of histological tissue analysis, single cell RNA sequencing and flow cytometry, we identified that mammary tissue from UTI-bearing mice display collagen deposition, enlarged ductal structures, ductal hyperplasia with atypical epithelial transcriptomes and altered immune composition. Bacterial cells were absent in the mammary tissue and blood of UTI-bearing mice, therefore, alterations to the distal mammary tissue were mediated by the systemic host response to local infection. Furthermore, broad spectrum antibiotic treatment resolved the infection and restored mammary cellular and tissue homeostasis. Systemically, unresolved UTI correlated with increased plasma levels of the metalloproteinase inhibitor, TIMP1, which controls extracellular matrix (ECM) remodeling and neutrophil function. Treatment of nulliparous and post-lactation UTI-bearing female mice with a TIMP1 neutralizing antibody, or broad-spectrum antibiotic, prevented mammary collagen deposition, thus providing evidence for an unexpected link between the systemic host response during UTI and mammary alterations.

Summary: The systemic response during urinary tract infection induces TIMP1-driven collagen deposition specifically into the mammary gland.

Introduction:

Alterations to the levels of whole body circulating factors in response to perturbations, such as infections and hormonal level variations, can influence bodily function in lasting ways¹⁻⁴. For example, while the onset of anemia may reduce the capacity of circulating oxygen, it also negatively alters organ functions by influencing cognitive function, chronic inflammation and immune responses to infection⁵. Similarly, bodily changes in response to persistent viral and bacterial infections, can result in pathological changes and excessive tissue damage, thus resulting in chronic diseases⁴. Interestingly, systemic alterations to a female body in response to hormonal changes especially during puberty and pregnancy result in lasting changes to mammary epithelial cell (MECs) maturation, mammary, liver and lung function, and immunity, thus representing whole body changes that positively influence tissue homeostasis^{6,7}.

Associations between bacterial pathogenesis and breast biology have been extensively studied in the context of mastitis, an infection process that has a negative impact on mammary health and lactation function⁸. However, little is known about how other whole-body responses induced by infections frequently experienced by women, such as those not local to the breast, affect breast health. One such concern that primarily afflicts women is urinary tract infections (UTIs), which affects one in three women globally⁹. UTIs elicit complex immunological host-responses as the body attempts to resolve the bacterial infection, by invoking local shedding of the urothelium, activation of resident innate immune cells, secretion of anti-microbial peptides, and systemic mobilization of innate and adaptive immune cells to the site of infection¹⁰. Here, we explored how the systemic host-response to bacterial urinary tract infection (UTI) induces tissue-specific alterations to mammary glands.

By utilizing a well characterized, clinically relevant, *in vivo* model of UTI in mice¹¹, we found that mammary tissue from UTI-bearing mice displayed ductal hyperplasia, altered adipocyte content, and abnormal collagen accumulation. UPEC bacterial cells were absent in the mammary tissue of UTI-bearing mice, suggesting that the observed tissue and cellular alterations were influenced by systemic host responses to infection, rather than localized infection. The onset of UTI also delayed mammary regression after lactation, marked by the presence of residual milk protein and non-regressed ductal structures, thus indicating the disruption of canonical cellular dynamics that control mammary function and homeostasis. Single cell RNA-sequencing (scRNA-seq) analysis illustrated that tissue alterations were accompanied by transcriptional changes in MECs, marked by upregulation of mechano-sensing programs. Such transcriptional alterations were associated with an altered communication between MECs and mammary fibroblasts, a finding that linked

distal infections (UTI) with mammary ECM, stroma, and epithelial alterations. Probing the circulatory factors elevated in UTI-bearing mice, we identified the Tissue Inhibitor of Matrix Metalloproteinases 1 (TIMP1): a regulator of ECM remodeling and turnover that inhibits several matrix-degrading proteases (Matrix Metalloproteinases or MMPs)^{12,13}. Preventing TIMP1 function with neutralizing antibody treatment during the course of infection fully restored mammary tissue homeostasis in UTI-bearing mice.

Collectively, our studies elucidate a mechanism by which a distal infection, commonly experienced by millions of women, can exert tissue-level effects beyond the local site, through modifying circulating factors. Our findings provide evidence for an expanded set of circulating factors, outside of hormones, that are induced by common life experiences and can have a profound effect on mammary biology and development, with relevance to potentially increasing the risk of future breast malignancy through collagen deposition driven changes to the stiffness of the tissue.

Results:

1. Mammary tissue homeostasis is altered in mice with unresolved UTI.

To study the impact of UTI on the mammary gland, we utilized a model system in which the bladders of female C57BL/6 mice were inoculated with the uropathogenic *E. coli* strain UTI89 (referred to hereafter as UTI mice)¹¹, or PBS (control mice), via transurethral delivery (**Fig. S1A**). The onset of UTI was confirmed at 48 hours post-infection (p.i.) with urine bacterial analysis (**Fig. S1B-C**). Mice that retained bacterial titers greater than 5×10^4 CFU/mL at 2 weeks p.i., signs of urothelial erosion, kidney immune infiltration, increased percentage of circulating granulocytes, and reduced percentage of circulating lymphocytes, were further analyzed (**Fig. S1D-H**). Infection retention phenotypes (urine bacterial titers, urothelial erosion, kidney immune infiltration) were absent at 2 weeks p.i. timepoint in control PBS mice, and UTI mice treated with broad-spectrum antibiotic, Trimethoprim-Sulfamethoxazole (hereafter referred to as TMS), which cleared UPEC from urine and resolved UTI, as previously demonstrated (**Fig. S1B-E**)^{14,15}. While the urine and bladder tissue were found positive for bacterial cells, analysis of total blood, plasma and mammary tissue from UTI-bearing mice failed to show bacteria, supporting that this is a model of localized bladder infection (**Fig. S1I-K**).

Analysis of mammary tissue from UTI-bearing mice revealed multiple mammary tissue abnormalities. H&E staining revealed expansion and enlargement of ductal structures in

mammary tissue from UTI-bearing mice, which were 80% more frequent and 154% bigger than mammary structures from PBS mice (**Fig. 1A-C**). Our analysis also indicated increased adipogenesis and collagen content in the mammary tissue from UTI-bearing mice, defined by an 14% increase of Perilipin+ adipocytes, and an 84% increase of collagen content than mammary tissue from PBS mice (**Fig. 1D-G**). Further analysis of collagen content with Picrosirius Red staining supported both thick and thin collagen fibers were at least 2-fold enriched in mammary tissue from UTI-bearing mice (**Fig. 1H-J**). Through analysis with two-photon microscopy and second harmonic generation (SHG) imaging, we found that the collagen present in the mammary gland of UTI-bearing mice displayed increased aligned architecture, suggesting that collagen accumulation could represent a combination of both altered synthesis/deposition and abnormal remodeling (**Fig. 1K-M**)¹⁶. Altered collagen deposition was not detected in other distal organs such as the pancreas, spleen, intestine, liver and lungs from UTI-bearing mice, suggesting that the ECM alterations resulting from unresolved UTI were specific in mammary gland tissue (**Fig. S2A**). We also found similar levels of corticosterone in the plasma of PBS control and UTI-bearing mice, suggesting that changes to this canonical regulator of infection responses and mammary tissue homeostasis does not represent the basis for UTI-associated changes to the gland (**Fig. S2B**).

An overall normalization of duct hyperplasia (197%), adipocyte counts (23%), and collagen content (41%) was observed in TMS treated animals, compared to non-TMS treated UTI-bearing animals, suggesting that tissue-level alterations induced by UTI are caused by the sustained host response to infection (**Fig. 1A-G**). Furthermore, TMS treatment of PBS control, healthy animals did not alter mammary collagen content, indicating that antibiotic treatment alone does not induce changes to the gland (**Fig. S2C-D**). We also investigated whether a short term exposure to UTI symptoms would induce mammary tissue alterations. In doing so female C57BL/6 mice were inoculated with uropathogenic strain, or PBS (control mice), via transurethral delivery, following UTI confirmation at 48 hours post-infection (p.i.) with urine bacterial analysis, and mammary tissue analysis at 72 hours p.i. (**Fig. S2E**). We found that mammary tissue from UTI-bearing mice compared to PBS controls at 72 hours p.i. showed no increase in ductal size or collagen deposition in UTI mice, suggesting that mammary alterations require sustained, systemic host-response during UTI (**Fig. S2F-I**). We also found similar plasma estrogen levels in UTI-bearing mice at 72 hours or 2 weeks p.i., further excluding abnormal levels of a master regulators of mammary tissue development as the basis for UTI-associated changes to the gland, and

supporting that mammary tissue changes in response to the onset of UTI are likely to be regulated by sustained responses to UTI (**Fig. S2J**).

2. The onset of UTI induces cellular and molecular alterations to mammary tissue.

Changes to mammary stroma composition have been linked with alterations to MEC lineage identity and gene regulation¹⁷⁻¹⁹. Therefore, we next employed scRNA-seq analysis to determine whether changes induced to mammary tissue in UTI-bearing mice resulted in alterations to epithelial cell abundance or transcriptional activity. In doing so, we generate scRNA-seq profiles of total mammary cells from UTI-bearing mice (2 weeks p.i.), and compared it to our previously published dataset generated from healthy, nulliparous mice (hereafter referred to as NP)²⁰.

Hierarchical clustering identified all 3 major epithelial lineages in mammary tissue from both healthy and UTI-bearing mice, including Basal-Myoepithelial cells (BM), Luminal adaptive secretory precursor cells (LASP), and Luminal hormone-sensing cells (LHS), with no statistically significant changes to cell abundance across health and UTI conditions (**Fig. 2A-B**)²¹. Interestingly, our analysis indicated the enrichment of MEC-ECM communication and mechano-sensing pathways in MECs from UTI-bearing mice (**S3A-B**). In fact, YAP networks, known canonical transducers and coordinators of transcription in response mechanical signals, such as from ECM deposition, were also found to be enriched in MECs from UTI-bearing mice, thus supporting alterations to MEC transcriptional states that associate with collagen deposition increase in response to UTI (**Fig. 2C**).

In the mammary gland, collagen remodeling is controlled throughout all major developmental stages, with fibroblasts playing a primary role in collagen synthesis, remodeling, and deposition²². Therefore, we next utilized our scRNA-seq datasets to investigate whether fibroblast abundance or inferred functions could be influencing MECs in UTI-bearing mice. In doing so, we performed a deep-cluster approach on cells expressing the stromal marker *Sparc* and lacking the expression of pan-epithelial marker (*Epcam*), pan-endothelial marker (*Pecam-1*) and pan-immune marker (*Ptprc*), as previously described^{23,24}. Such approach identified 3 populations of fibroblasts (referred hereafter as Nulliparous fibroblasts, NPF), from which cluster NPF2 was defined to be significantly enriched in samples from UTI-bearing mice (**Fig. S3C-D**). Differentially expressed analysis of gene markers indicated that fibroblasts enriched in mammary tissue from UTI-bearing mice (NPF2) is defined by high expression of genes that are associated with ECM/collagen remodeling such as *Myoc*, *Ogn*, *Hmgn2*, and *Thbs4* (**Fig. S3E**)²⁵⁻²⁸. In agreement, additional analysis of fibroblast lineage state indicated that NPF2 cells showed signatures of fibroblasts

described to have a higher collagen synthesis potential, thus further supporting that an ongoing UTI stimulates the presence of fibroblasts with collagen related functions in the mammary gland (**Fig. 2D**)²⁹. This was in marked contrast to fibroblasts subtypes also present in mammary tissue from healthy animals, which were classified as immuno-regulatory-like states (NPF1), and myofibroblasts (NPF3) (**Fig. 2D**). In fact, immune staining analysis of Fibronectin levels, an extracellular matrix protein that interacts with collagen, and highly expressed in NPF2 fibroblasts, confirmed increased abundance of Fn1+ stromal cells around mammary gland structures of UTI-bearing mice, thus further supporting that an ongoing UTI stimulates the presence of fibroblasts with collagen related functions in the mammary gland (**Fig. 2D, red asterix, and 2E**). Collectively, our analysis so far suggests that structural changes to mammary tissue in UTI-bearing mice (collagen deposition) are influencing the transcriptional state of MECs, and the abundance of collagen-associated cell types (fibroblasts).

We next asked whether we could infer a direct communication between MECs and fibroblasts in mammary tissue from UTI-bearing mice, using CellChat analysis of scRNA-seq datasets from the mammary gland of control and UTI-bearing mice³⁰. We found stronger emission of ECM related signals, specifically collagen and laminin ones, by NPF2 fibroblasts present in the mammary tissue of UTI-bearing mice to major MEC subtypes, compared to signal sent by NPF1 fibroblasts, which is present in tissue from both healthy and UTI-bearing mice (**Fig. 2F-G and S3F-G**). Further analysis of receptor-ligand pairs predicted that *Itga9-Itgb1* pairing was predominant between NPF1 and NPF2 fibroblasts, and major MEC subtypes in the mammary tissue of UTI-bearing mice, while *Itgav-Itga8* pairing was more frequent between NPF1 fibroblasts and MECs in the non-UTI mammary tissue (**Fig. 2H-I**). Interestingly, *Itga3-Itgb1* pairing, which was predicted to be in place across conditions between fibroblasts and BM cells, was also more frequent between fibroblasts and LHS cell types in UTI-bearing mice (**Fig. 2H-I**). Collectively, this analysis provides *in silico* support of signaling mechanisms associated with specific subtypes of fibroblasts and receptor-ligand pairing that are altered in UTI-bearing mice, and associate with the increased mammary collagen accumulation.

3. UTI interferes with mammary gland involution post-lactation

Post-partum women are at increased risk to develop recurrent and difficult to treat UTIs³¹. Having characterized the effects of unresolved UTI on mammary tissue homeostasis in nulliparous mice, we next investigated whether a critical timepoint of mammary gland development, the resolution of pregnancy-induced changes that occur during post-partum tissue involution would be impacted in UTI-bearing mice. In doing so, we analyzed the mammary tissue of actively nursing female

mice (full-term pregnancy, 10 days of nursing) post transurethral delivery of either UTI89 uropathogenic bacteria (UTI condition) or PBS control. After confirmation of bacteriuria, 48 hrs p.i., the offspring were weaned to induce forced mammary involution. Bacteriuria and tissue analysis were conducted 10 days post-lactation involution (referred hereafter as PLI), a time-point at which the mammary gland is expected to have significantly regressed to its pre-pregnancy state (**Fig. S4A**)³². UTI-bearing PLI mice 2 weeks p.i. showed bacteria titers, bladder and kidney alterations similarly to the ones observed in nulliparous mice, relative to PBS controls, thus indicating the onset of UTI and associated host response (**Fig. S4B-C**).

Analysis of mammary tissue from UTI-bearing PLI mice revealed mammary tissue abnormalities. H&E staining revealed increased number of ductal structures in the mammary tissue of UTI-bearing PLI (black arrows), which we confirmed with immunofluorescent image analysis, and indicated a 76% increase on the number of ductal structures (defined by Cytokeratin 5 staining) (**Fig. 3A-C**). H&E tissue analysis of mammary tissue from UTI-bearing PLI mice also suggested increased milk accumulation into the ducts, which we investigated with the quantification of the milk-associated protein β -casein, an analysis that revealed a 733% increase of β -casein signal, relative to PBS control, suggesting that unresolved UTI impacts on the post-lactation process of the mammary gland (**Fig. 3D**).

We also identified that mammary tissue from UTI-bearing PLI mice displayed a statistically significant, 24% increase in collagen content, compared to PBS control, an alteration also present in the tissue of nulliparous (never pregnant) mice, thus suggesting collagen alterations that are brought by the onset of UTI to mammary gland that are independent of parity (**Fig. 3E-F and S4D**). Analysis of adipocyte content, a cell type that disappears from the mammary tissue during pregnancy³³, but is reestablished early during post-lactation involution, showed a subtle, but non-statistically significant, cellular expansion in UTI-bearing PLI mice (**Fig. S4E-F**). Collectively, these findings suggest that during active tissue remodeling phase, as observed during the transition from lactation to involution, UTI-induced mammary alterations result in milk-accumulation and collagen deposition.

We next performed scRNA-seq analysis, to further investigate the impact of an ongoing UTI on cellular and molecular states of mammary tissue undergoing post-lactation involution. Our analysis identified all major MEC lineages (BM, LASP, and LHS), which were equally distributed in abundance across UTI and PBS conditions (**Fig. S5A-B**). We found that pathways linked with YAP-signaling signatures were also enriched in several MECs lineages from UTI-bearing mice, once again illustrating changes that influenced both never pregnant and involuting mammary

tissue (**Fig. 3G**). Differential transcriptional analysis indicated that pathways associated with the transition between lactation and early steps of involution, such as IL2-Stat5 and TNF α signaling, were enriched in LASPs from PLI UTI-bearing mice, suggesting a yet to be fully initiated involution process (**Fig. 3H**). Interestingly, some of genes associated with such pathways were up-regulated across all MECs, thus suggesting that a signature of partial involution initiation was shared by all epithelial cells in UTI-bearing mice (**Fig. S5C**). In contrast, LASPs from PLI PBS control animals, were enriched with processes linked with active process of involution and immune recruitment, such as IL6/Stat3 and IFN γ responses, suggesting a molecular signature of ongoing involution (**Fig. 3H**). Collectively, these observations suggest that molecular processes associated with the progress through involution were not fully activated in LASPs from PLI UTI-bearing mice, a finding that supports the observation of milk protein residue accumulation, and further suggests that the onset of UTI delays the post-lactation involution of mammary tissue.

The balance between YAP-signaling, collagen content, milk production is of extreme importance during lactation and involution. While collagen provides the environment for expansion and specialization of milk producing cells (LASPs) and contractile cells (BMs), the increased collagen provides the orientation for tissue wound healing during removal of dead cells during involution^{34,35}. Such increased collagen concentration during involution is induced by specific subtypes of fibroblasts²⁹. Our analysis of nulliparous tissue indicated that collagen and MEC transcriptional alterations in UTI-bearing mice were associated with specific subtypes of fibroblasts (**Fig. 2E-H**). Therefore, we next investigated whether specific populations of fibroblasts were more abundantly present in the mammary tissue from UTI-bearing PLI mice.

Through this analysis, we identified 2 fibroblast clusters (referred here after as post-lactation fibroblasts, PLIF), which we defined as distinct states of mammary fibroblasts according to the enrichment of collagen remodeling genes (PLF1) and myofibroblasts associated genes (PFLI2) (**Fig. S5D-F**). Unlike the observation of nulliparous UTI-bearing mice, we did not detect changes to the fibroblast abundance comparing UTI and PBS conditions, nor identified a nulliparous-like Fn1+ fibroblast signature, suggesting during post-lactation involution such fibroblast state is less common, and that the onset of UTI did not majorly alter already in place fibroblast identities (**Fig. S5F**). We also found that fibroblasts of both PBS control and UTI-bearing PLI mice expressed similar levels of fibroblast activated genes, suggesting that UTI processes did not perturb signatures associated with those induced by involution (**Fig. 3I**)³⁵. Prediction of collagen signaling, and overall communication between fibroblasts and MECs in PLI animals, indicated an overall overlap of signals being sent by fibroblasts to MECs across UTI-bearing and PBS conditions (**Fig.**

3J-K and S5G-H). Taken together, these findings support that UTI-induced alteration to the mammary tissue during post-lactation involution are not as prominent as the ones encountered in nulliparous animals.

4. UTI induces infiltration of neutrophils into the mammary gland independent of systemic CSF3

UTIs elicit complex immunological host-responses, with the recruitment of specific immune cells, both locally to the bladder and systemically, as the body attempts to counter the bacterial infection^{36,37}. Our initial findings indicated a sustained elevation of granulocytes in the circulation of UTI-bearing mice, as one of the symptoms that persisted 2 weeks p.i. (**Fig. S1**). In fact, and in addition to programs activated by collagen and ECM, our scRNA-seq datasets indicated that MECs from nulliparous UTI-bearing mice were also enriched for genes linked with neutrophil recruitment, suggesting that the elevated levels of neutrophils in the blood could be sensed by the mammary tissue (**Fig. 4A**). Interestingly, neutrophil recruitment signature was downregulated in MECs from UTI-bearing PLI mice, perhaps suggest that such mechanism is differentially modulated according to the state of mammary gland development (**Fig. S6A**). We therefore, set out to validate whether neutrophils were indeed recruited to the mammary gland in response to an ongoing UTI.

Flow cytometry analysis indicated a 93% increase in the abundance of total CD45⁺, CD11b^{hi}Ly6G⁺ neutrophils in mammary glands from UTI-bearing mice, compared to PBS mice, a population of immune cells that has been described to be expanded in order to attenuate inflammatory responses (**Fig. 4B**)³⁸. We did not detect changes to the abundance of CD11b^{hi}Ly6G⁻ myeloid cells (**Fig. 4C**)³⁹. Neutrophils recruited to mammary tissue returned to normal levels upon treatment of UTI-bearing mice with TMS, suggesting that neutrophil expansion in the mammary tissue is driven by changes triggered during ongoing UTI (**Fig. 4B-C**). Analysis of an earlier time-point during the course of UTI (72 hours p.i.) showed no significant difference in the abundance of neutrophils in mammary tissue, suggesting that the alterations observed in the gland at 2 weeks p.i. were a consequence of the sustained responses to UTI (**Fig. S6B-C**). We also did not find differences in the population of neutrophils across UTI and PBS conditions at 2 weeks p.i. in PLI mice, a finding that agrees with the levels of neutrophil recruitment signature detected in MECs (**Fig. S6D**).

To understand if neutrophil recruitment during UTI was mammary-specific, we evaluated multiple tissues across the body at 2 weeks p.i.. In doing so, we utilized immunofluorescence staining to detect the neutrophil marker, myeloperoxidase (Mpo+). This analysis indicated Mpo+ cells in the

mammary tissue of UTI-bearing mice, supporting the flow cytometry expansion of this population of cells (**Fig. 4D, red label**). We also found that Mpo⁺ neutrophils in the mammary of UTI-bearing mice did not express high levels of citrullinated histone H3 (cit. H3), suggesting the lack of neutrophil extracellular traps (NETs) as a consequence of neutrophil recruitment to the mammary gland during UTI (**Fig. 4D, green label**)⁴⁰. Additional analysis indicated increased Mpo⁺ neutrophils in the spleen, pancreas, lung and liver of UTI-bearing mice, with no statistically differences in the bone marrow and intestines comparing UTI to PBS conditions (**Fig. S6E-F**). This finding suggests that the neutrophil infiltration varies across tissues in UTI-bearing mice, and it is not exclusive to mammary tissue.

Given that increased levels of granulocytes are part of the systemic response to a UTI (**Fig. S1**), we sought to identify the circulatory factors regulating the mammary-specific phenotypes in UTI-bearing mice⁴¹. Unbiased analysis of plasma cytokines identified elevated levels of Granulocyte colony stimulation factor (G-CSF, 62-fold) and Chemokine (C-X-C) motif ligand 1 (CXCL1, 4-fold), known granulocyte-associated factors in the plasma of UTI-bearing mice (**Fig. 4E**)^{12,42}. We also found elevated levels of Tissue inhibitor of matrix metalloproteinases 1 (TIMP1, 3-fold), a factor previously shown to regulate neutrophilia and collagen remodeling, in the plasma of UTI-bearing mice (**Fig. 4E**)^{12,42}. To confirm that the systemic host response to unresolved UTI is sufficient to drive granulocyte proliferation in a reductionist setting, we cultured total bone marrow cells from healthy mice with plasma from UTI-bearing mice. We found that culture supplementation with plasma from UTI-bearing mice induced a 41% expansion of granulocytes, in comparison to cultures treated with plasma from PBS mice (**Fig. S6G**). This effect was exclusive to granulocytic cells, given that the abundance of monocytes remained unchanged across the culturing conditions (**Fig. S6H**). These findings support the notion that systemic host responses to UTI is accompanied by the increase in many granulocyte-stimulating factors in the circulating plasma, which induce granulocyte expansion *in vivo* and *in vitro*.

We next set out to define whether the UTI-induced factor and canonical driver of neutrophil expansion, G-CSF (also known as CSF3), contributed to the expansion of neutrophils in the mammary gland. In doing so, we utilized a previously established protocol, to treat UTI-bearing mice with either control IgG or CSF3 neutralizing antibodies (referred to hereafter as anti-CSF3) by intraperitoneal injection for 2 weeks starting 48 hours after UTI establishment (**Fig. S6I**)⁴³. This treatment did not change the severity of UTI infection, given that both IgG and anti-CSF3 treated UTI-bearing mice continued to display high levels of bacteria in the urine, and histological signs of unresolved infection (**Fig. S6J-K**). Evaluation of blood and mammary tissue indicated that anti-

CSF3 treatment did not impact the abundance of mammary or circulating CD11b^{hi} Ly6G⁺ neutrophils, indicating that during an ongoing UTI, inhibition of CSF3 alone is not sufficient to resolve elevated levels of neutrophils (**Fig. 4F-G and S6L-N**). Intriguingly, we found a 58% reduction of collagen in the mammary gland of UTI-bearing mice treated with anti-CSF3, relative to IgG treated animals, indicating a link between neutrophil-inducing factors and collagen accumulation (**Fig. 4H-I**). In fact, anti-CSF3 treatment has been previously demonstrated to alleviate collagen-induced arthritis, and to control the differentiation and proliferation of fibroblasts, major collagen producers in the mammary gland and more abundant in the tissue of UTI-bearing mice (**Fig. 2**)⁴⁴. Overall, our findings suggest that multiple UTI-associated factors may play a role in controlling collagen production in mammary tissue.

5. Neutralization of TIMP1 levels in UTI-bearing mice restores mammary homeostasis in nulliparous and post-parous mice.

While CSF3 neutralization did reduce collagen accumulation in nulliparous UTI-bearing mice, it did not change mammary neutrophil recruitment, indicating a bi-modal role on immune and collagen-producing cell types during an ongoing UTI (**Fig. 4H-I**). Interestingly, a more classical collagen remodeling factor, TIMP1, was also more abundant in the plasma of UTI-bearing mice (**Fig. S7A-B**). Since TIMP1 is a known regulator of mammary collagen accumulation, involution progression, and adipocyte content, all relevant to phenotypes observed in UTI-bearing animals, we next tested whether neutralization of TIMP1 levels would restore UTI-induced mammary alterations^{13,45–48}.

In doing so, we utilized previously published protocols, and treated nulliparous UTI-bearing mice with either control IgG or TIMP1 neutralizing antibodies (referred to hereafter as anti-TIMP1) (**Fig. S7C**)⁴⁹. TIMP1 neutralization did not alter the severity of UTI, as demonstrated by similar levels of bacteriuria, histopathological abnormalities in the bladders and kidneys of UTI-bearing animals (**Fig. S7D-E**). Treatment with anti-TIMP1 decreased the levels of plasma TIMP1 by 10-fold in UTI mice, in addition to lowering the levels of CSF3 (14-fold) as compared to the isotype control, confirming a co-regulation of circulating factors that respond to UTI (**Fig. S7F**).

Histological analyses of anti-TIMP1 treated mice indicated normalization of mammary tissue phenotypes, with a 74% reduction in duct size, a 15% decrease in the abundance of Perilipin⁺ adipocytes, and a 39% decrease in the amount of collagen content, compared to IgG-treated mice (**Fig. 5A-F**). After further characterization of the collagen content of IgG control and anti-TIMP1 treated UTI-bearing mice with SHG, which confirmed the reduction in collagen deposition upon anti-TIMP1 treatment, we discovered that TIMP1 neutralization was sufficient to prevent

increased collagen alignment observed previously in mammary tissue from UTI-bearing mice (**Fig. 5G-I**). Alongside rescuing UTI-driven mammary-specific ECM remodeling, TIMP1 neutralization also decreased the abundance of mammary infiltrating CD11b^{hi}Ly6G⁺ neutrophils by 53% compared to control IgG-treated UTI-bearing mice, in contrast to other circulating and mammary infiltrating immune cells populations, which remained unchanged (**Fig. 5J and S7G**). There was no significant difference in the levels of estrogen between the control IgG and anti-TIMP1-treated UTI mice, further supporting that TIMP1, and no other circulating factors that can impact neutrophil homing, drove the alterations to the mammary tissue in UTI-bearing mice (**Fig. S7H**)^{50,51}.

We also evaluated the importance of TIMP1 in coordinating mammary tissue changes by applying the same TIMP1 neutralization regimen in UTI-bearing PLI mice (**Fig. S8A**). TIMP1 neutralization did not alter the severity of UTI, as demonstrated by similar levels of bacteriuria, histopathological abnormalities in the bladders and kidneys between UTI-bearing mice in both treatment groups (**Fig. S8B-C**). Treatment with anti-TIMP1 decreased the levels of plasma TIMP1 by 6.1-fold in UTI-bearing anti-TIMP1 mice, in addition to lowering the levels of G-CSF by 2.8 fold as compared to the isotype control (**Fig. S8D**).

Treatment with anti-TIMP1, similarly to the nulliparous context, reduced mammary collagen deposition by 63% in UTI-bearing mice PLI, relative to controls, (**Fig. 5K-L**). However, anti-TIMP1 did not reverse phenotypes associated with involution processes. TIMP1 neutralization did not ameliorate the delay in involution phenotype in UTI-bearing post-lactation mice, based on similar levels of Cytokeratin 5+ signal (duct content) and β -casein staining (milk residue), relative to IgG isotype control treated mice (**Fig. S8E-G**). Additionally, TIMP1 neutralization did not reduce the number of adipocytes induced by UTI in the PLI model when compared to controls (**Fig. S8H-I**) nor the abundance of circulating or mammary neutrophils and circulating monocytes, all of which were unchanged relative to controls (**Fig. S8J-M**).

Collectively, these data support that TIMP1 serves as a critical factor, mediating the influence of the systemic UTI-host-response on mammary ECM remodeling, controlling phenotypes in both nulliparous and post-lactation physiologic contexts. In summary, these data provide evidence for an unappreciated role for how the host response to a localized infection can change the cellular and tissue homeostasis of a distal organ, the mammary gland.

Discussion.

In this study, we demonstrated for the first time that UTI-elicited host-responses, largely mediated

by increased systemic TIMP1 levels, drive mammary tissue disorganization, alter cellular abundances, and impact the transcriptional programs of MECs as a response to tissue microenvironment changes.

Using models of induced and treatable infection, we were able to recapitulate clinically relevant UTI etiology and pathobiology in mice. With this model, we demonstrated that the UTI's influence on the mammary tissue was independent of bacterium translocation from the bladder to the mammary tissue, but rather acting through induced systemic effectors^{8,52}. This observation alone suggests against the possibility that our analysis investigated a mastitis-associated phenotype, an infection of breast tissue commonly observed in post-partum women, which is associated with *E.coli* mammary colonization and local tissue inflammatory signals. It is worth noting that our study did not address changes to the mammary local microbiota that may occur in response to an ongoing UTI, which could also play a role in impacting tissue metabolism, development, and immunity^{53,54}. Nonetheless, inhibition of UTI-induced circulatory factors, specifically TIMP1, restored mammary tissue health, thus suggesting a master regulator on mammary dynamics in response to the onset of UTI.

Bacterial antigens and bacteria-induced tissue damage triggers chemotactic signals that activate and recruit neutrophils to the infected tissue³⁶. Neutrophil stimulating cytokines like G-CSF and CXCL1 are induced in the bladder tissue within 6 hours of a UTI, and our results demonstrated that such levels remain elevated 2 weeks post UTI infection^{36,43,55}. While our transcription analysis indicated enrichment of neutrophil recruitment signals on MECs from UTI-bearing mice, a broader analysis indicated expanded neutrophil homing across many other tissues, thus ruling out that neutrophil infiltration during ongoing UTI is mammary specific. Interestingly, targeting of G-CSF, a master regulator of neutrophil release from the bone marrow and tissue homing, with neutralizing antibodies did not impact with overall neutrophil levels, but instead substantially decreased the accumulation of collagen in mammary tissue⁵⁶. In fact, G-CSF has been associated with increased expression of collagen genes and alleviating collagen-induced arthritis, thus supporting its multi-functional role regulating mammary phenotypes during an ongoing UTI⁵⁷. Moreover, and given G-CSF also plays a role on regulating the proliferation and differentiation of fibroblasts, these observations support our findings that specific, collagen-producing fibroblast are expanded in nulliparous UTI-bearing mice, further indicating a possible feedback loop of signals that control neutrophil trafficking and collagen remodeling in the mammary gland.

Our findings also illustrated that the MECs responded to the UTI-induced factors in a mammary developmental context-dependent manner. While mechano-sensing and neutrophil recruitment transcriptional programs were altered in major MEC lineages across mammary developmental stages, UTI during post-lactational involution associated with LASP populations expressing signals of both lactation and involution process, a conclusion also supported by tissue analysis. While such signals of delayed involution may be influenced by combinatorial systemic responses to UTI, changes to mammary microenvironment, and overall cellular states, it illustrates that infections that women are at a higher risk to develop during and after pregnancy could impact the usually tightly controlled process of tissue reconstruction post-lactation. Interestingly, disruption of post-pregnancy/lactation tissue remodeling may provide a niche for oncogenic initiation and malignant outgrowth, and therefore representing a possible alteration that contributes to the incidence of post-partum breast cancer^{58,59}.

The UTI-elicited alteration of the mammary ECM was reflected in the excessive accumulation of collagen within the mammary fat-pad, along with the presence of increasingly aligned collagen fibers. Increased collagen content within the mammary gland has been described to increase the inherent elasticity of tissues, resulting in increased stiffness of the underlying tissue, with subsequent impact on the proliferation, differentiation and lineage commitment of the neighboring epithelial cells, through stimulation of pro-survival, mechano-sensing pathways¹⁷. Therefore, the activation of such transcriptional programs, as shown on our scRNA-seq analysis, along with the collagen accumulation affecting tissue stiffness, are features that could create a pro-tumorigenic microenvironment and generate windows of opportunities for the development and progression of malignance within a tumorigenic niche, across developmental stages of the gland^{17,60}.

But most importantly, our study elucidated the link between TIMP1 levels, mammary tissue alterations, and an ongoing UTI. Increased TIMP1 levels has been associated with granulopoiesis, neutrophilia, and collagen accumulation and altered adipogenesis in several tissues, including but not limited to the mammary gland, cardiac tissue, lungs and kidneys^{12,17,42,61-63}. In the mammary gland, prolonged expression of TIMP1 has been shown to impair post-lactation regression of ductal structures, and persistent milk production, therefore matching the phenotype observed in UTI-bearing mice during post-lactation involution^{45,48}. Here, utilizing a neutralizing antibody approach targeting TIMP1, we were able to fully rescue the abnormal neutrophil infiltration, adipocyte expansion, ductal abnormality, and collagen deposition in the mammary tissue of UTI-bearing mice. TIMP1 neutralization restored homeostasis in the mammary gland in UTI-bearing mice without affecting disease presentation in the bladder or

kidney or impacting circulating estrogen or corticosteroids levels, supporting that its mammary-specific impact is central to the influence of UTI on mammary health and demonstrates the organ-specific connection between distal infection, host response, and mammary abnormalities. While in post-lactating UTI-bearing mice TIMP1 neutralization only corrected mammary collagen accumulation, targeting TIMP1 levels in nulliparous animals resolved mammary tissue architecture and cellular composition of UTI-bearing. Therefore, our findings support a master regulatory role for TIMP1 on controlling mammary homeostasis, when induced by the infection response, and the link between mammary health and systemic responses to distal infections.

But where does TIMP1 come from in UTI-bearing mice? TIMP1 has predominantly been detected in polymorphonuclear cells and resident tubular cells in the kidneys, suggesting that both polymorphonuclear cells, like neutrophils, and tissue-derived TIMP1 could contribute to the increased pool of TIMP1 in circulation in UTI-bearing mice⁶⁴. While our analyses did not differentiate between TIMP1 proteins bound to the neutrophil surface or actively secreted by neutrophil subtypes, the elevation of TIMP1 levels in the plasma of UTI-bearing mice supports that it is secreted into circulation⁶⁵.

Our findings illustrate a new paradigm in mammary biology and development as they show that the plasticity of the mammary gland, canonically thought to be largely hormone-responsive, can also be modulated by other common health events, such as infection. The changes we observe in the mammary gland during an ongoing UTI bear relevance to breast density and fibrosis, changes that have the potential to foreshadow increased risk of future malignancy. This suggests that other systemic events in a woman's life, outside of female hormones and age, should be considered with respect to how they impact breast health, especially in populations at risk for developing breast cancer such as from germline mutations or lifestyle factors. The further relevance of these UTI-induced changes within mammary tissue to potential future breast oncogenesis should be studied further in mouse models of breast cancer and evaluated with large scale epidemiological datasets.

Methods

Animals. Nulliparous and timed-pregnant (gestation day E11-E15), female, C57BL/6J mice were purchased from The Jackson Laboratory. All animals were housed at the CSHL shared Laboratory Animal Resource under a 12 hr. light/dark cycle, with controlled temperature and humidity at 72°F and 40-60%, respectively, and with access to dry food and water ad libitum, unless otherwise specified. All animal experiments were performed in accordance with CSHL Institutional Animal Care and Use Committee guidelines. All animal related analysis (UTI,

offspring weaning, and treatments) were performed as described in Supplemental Experimental Procedures.

Tissue collection and processing for histological analyses. Mammary gland (left inguinal), bladder, kidney, spleen, lungs, liver, intestines, and pancreas were harvested at the experimental endpoint and immediately fixed in 4% paraformaldehyde in 1X PBS (16% solution, Electron Microscopy Sciences, cat# 15711) at 4°C overnight, followed by storage in 1X PBS at 4°C, until paraffin embedding. Tissue processing, paraffin embedding, sectioning, staining, digestion and analysis were performed as described in Supplemental Experimental Procedures.

RNA sequencing (scRNA-seq) library preparation and analysis. scRNA-seq libraries were prepared, normalized, integrated, batch corrected and analyzed as described in Supplemental Experimental Procedures.

Funding. This work was performed with the support by the CSHL and Northwell health affiliation (C.O.D.S.), the Pershing Square Sohn Prize for Cancer Research (C.O.D.S.), the Robertson foundation, the NIH/NCI grant R01CA248158-01 (C.O.D.S.), NIH/NIA grant R01 AG069727-01 (C.O.D.S.), the NIH/NCI 1R01CA284630 (C.O.D.S.), the NIH NCI grant F30CA281082 (S.M.L.), the NIHGM T32GM008444 (S.M.L.), and the NIH NCI grant 1R01CA2374135 (M. E.). CSHL Cancer Center Shared Resources are supported by the CSHL Cancer Center Support Grant 5P30CA045508

Author contributions. Conceptualization: C.O.D.S.; Methodology: S.H., S.M.L., S.L.C., M.K.C., A.V.H.S., G.J., D.C., X.H., M.F.C., I.A.D., A.B., D.C., E.H., T.H., D.T., and M.E.; Investigation: S.H., S.M.L., S.L.C., M.K.C., G.J., E.H., J.E.W., Visualization: S.H., S.M.L., S.L.C., M.K.C., X.H. Funding acquisition: C.O.D.S.; Project administration: C.O.D.S.; Supervision: C.O.D.S.; Writing – original draft: C.O.D.S, S.L.C., S.H. and S.M.L. Writing – revised draft: C.O.D.S, S.H. and S.M.L.

Acknowledgements: We thank the CSHL Cancer Center Shared Resources (Laboratory Animal Resource, Histology, Microscopy, Flow Cytometry and Single Cell Sequencing core facilities) for their assistance in the completion of the described study and the entire dos Santos lab for their insights and helpful discussions related to this manuscript.

Declaration of Interests. The authors have no competing interests to disclose.

Data and Materials Availability. scRNA-seq were deposited into BioProject database under number SUB11741283, and will be publicly available as of the date of publication. All accession numbers are listed in Table M1-2 (supplementary methods). Results datasets used on Fig. 2 and

- 10 Bowyer GS, Loudon KW, Suchanek O, Clatworthy MR. Tissue Immunity in the Bladder. *Annu Rev Immunol* 2022;**40**:499–523. <https://doi.org/10.1146/annurev-immunol-101220-032117>.
- 11 Hung CS, Dodson KW, Hultgren SJ. A murine model of urinary tract infection. *Nat Protoc* 2009;**4**:1230–43. <https://doi.org/10.1038/nprot.2009.116>.
- 12 Kobuch J, Cui H, Grünwald B, Saftig P, Knolle PA, Krüger A. Timp-1 signaling via CD63 triggers granulopoiesis and neutrophilia in mice. *Haematologica* 2015;**100**:1005–13. <https://doi.org/10.3324/haematol.2014.121590>.
- 13 Arpino V, Brock M, Gill SE. The role of TIMPs in regulation of extracellular matrix proteolysis. *Matrix Biol* 2015;**44–46**:247–54. <https://doi.org/10.1016/j.matbio.2015.03.005>.
- 14 O'Brien VP, Hannan TJ, Yu L, Livny J, Roberson EDO, Schwartz DJ, *et al*. A mucosal imprint left by prior Escherichia coli bladder infection sensitizes to recurrent disease. *Nat Microbiol* 2016;**2**:. <https://doi.org/10.1038/nmicrobiol.2016.196>.
- 15 Yu L, O'Brien VP, Livny J, Dorsey D, Bandyopadhyay N, Colonna M, *et al*. Mucosal infection rewires TNF α signaling dynamics to skew susceptibility to recurrence. *Elife* 2019;**8**:20–30. <https://doi.org/10.7554/eLife.46677>.
- 16 Liu Y, Keikhosravi A, Mehta GS, Drifka CR, Eliceiri KW. *Methods for Quantifying Fibrillar Collagen Alignment*. 2017.
- 17 Schedin P, Keely PJ. Mammary gland ECM remodeling, stiffness, and mechanosignaling in normal development and tumor progression. *Cold Spring Harb Perspect Biol* 2011;**3**:1–22. <https://doi.org/10.1101/cshperspect.a003228>.
- 18 Rauner G, Kuperwasser C. Microenvironmental control of cell fate decisions in mammary gland development and cancer. *Dev Cell* 2021;**56**:1875–83. <https://doi.org/10.1016/j.devcel.2021.06.016>.
- 19 Hayward MK, Muncie JM, Weaver VM. Tissue mechanics in stem cell fate, development, and cancer. *Dev Cell* 2021;**56**:1833–47. <https://doi.org/10.1016/j.devcel.2021.05.011>.
- 20 Henry S, Trousdell MC, Cyrill SL, Zhao Y, Feigman MJ, Bouhuis JM, *et al*. Characterization of Gene Expression Signatures for the Identification of Cellular Heterogeneity in the Developing Mammary Gland. *J Mammary Gland Biol Neoplasia* 2021;**26**:43–66. <https://doi.org/10.1007/s10911-021-09486-3>.
- 21 Phipson B, Sim CB, Porrello ER, Hewitt AW, Powell J, Oshlack A. Propeller: Testing for

- Differences in Cell Type Proportions in Single Cell Data. *Bioinformatics* 2022;**38**:4720–6. <https://doi.org/10.1093/bioinformatics/btac582>.
- 22 Plikus M V., Wang X, Sinha S, Forte E, Thompson SM, Herzog EL, *et al.* Fibroblasts: Origins, definitions, and functions in health and disease. *Cell* 2021;**184**:3852–72. <https://doi.org/10.1016/j.cell.2021.06.024>.
- 23 Bartoschek M, Oskolkov N, Bocci M, Lövrot J, Larsson C, Sommarin M, *et al.* Spatially and functionally distinct subclasses of breast cancer-associated fibroblasts revealed by single cell RNA sequencing. *Nat Commun* 2018;**9**:. <https://doi.org/10.1038/s41467-018-07582-3>.
- 24 Kanaya N, Chang G, Wu X, Saeki K, Bernal L, Shim HJ, *et al.* Single-cell RNA-sequencing analysis of estrogen- and endocrine-disrupting chemical-induced reorganization of mouse mammary gland. *Commun Biol* 2019;**2**:1–15. <https://doi.org/10.1038/s42003-019-0618-9>.
- 25 Ueda J, Yue BYJT. Distribution of Myocilin and Extracellular Matrix Components in the Corneoscleral Meshwork of Human Eyes. *Investig Ophthalmol Vis Sci* 2003;**44**:4772–9. <https://doi.org/10.1167/iovs.02-1002>.
- 26 Nulali J, Zhan M, Zhang K, Tu P, Liu Y, Song H. Osteoglycin: An ECM Factor Regulating Fibrosis and Tumorigenesis. *Biomolecules* 2022;**12**:. <https://doi.org/10.3390/biom12111674>.
- 27 Lin MH, Pope BD, Sasaki T, Keeley DP, Sherwood DR, Miner JH. Mammalian hemicentin 1 is assembled into tracks in the extracellular matrix of multiple tissues. *Dev Dyn* 2020;**249**:775–88. <https://doi.org/10.1002/dvdy.159>.
- 28 Stenina-Adognravi O, Plow EF. Thrombospondin-4 in tissue remodeling. *Matrix Biol* 2019. <https://doi.org/10.1016/j.matbio.2017.11.006>.Thrombospondin-4.
- 29 Guo Q, Minnier J, Burchard J, Chiotti K, Spellman P, Schedin P. Physiologically activated mammary fibroblasts promote postpartum mammary cancer. *JCI Insight* 2017;**2**:1–18. <https://doi.org/10.1172/jci.insight.89206>.
- 30 Jin S, Guerrero-Juarez CF, Zhang L, Chang I, Ramos R, Kuan CH, *et al.* Inference and analysis of cell-cell communication using CellChat. *Nat Commun* 2021;**12**:1–20. <https://doi.org/10.1038/s41467-021-21246-9>.
- 31 Denoble A, Reid HW, Krischak M, Rosett H, Sachdeva S, Weaver K, *et al.* Bad bugs: antibiotic-resistant bacteriuria in pregnancy and risk of pyelonephritis. *Am J Obstet Gynecol MFM* 2022;**4**:1–17. <https://doi.org/10.1016/j.ajogmf.2021.100540>.

- 32 Tsutsui S, Wakasa H, Tsugami Y, Suzuki T, Nishimura T, Kobayashi K. Distinct Expression Patterns of Fibrillar Collagen Types I, III, and V in Association with Mammary Gland Remodeling during Pregnancy, Lactation and Weaning. *J Mammary Gland Biol Neoplasia* 2020;**25**:219–32. <https://doi.org/10.1007/s10911-020-09457-0>.
- 33 Wang QA, Scherer PE. Remodeling of Murine Mammary Adipose Tissue during Pregnancy, Lactation, and Involution. *J Mammary Gland Biol Neoplasia* 2019;**24**:207–12. <https://doi.org/10.1007/s10911-019-09434-2>.
- 34 Maretová E, Maretta M. The Distribution of Collagen and Elastic Fibres in the Lactating Bovine Mammary Gland. *Folia Vet* 2019;**63**:60–5. <https://doi.org/10.2478/fv-2019-0028>.
- 35 Guo Q, Sun D, Barrett AS, Jindal S, Pennock ND, Conklin MW, *et al.* Mammary collagen is under reproductive control with implications for breast cancer. *Matrix Biol* 2022;**105**:104–26. <https://doi.org/10.1016/j.matbio.2021.10.006>.
- 36 Ching C, Schwartz L, Spencer JD, Becknell B. Innate immunity and urinary tract infection. *Pediatr Nephrol* 2020;**35**:1183–92. <https://doi.org/10.1007/s00467-019-04269-9>.
- 37 Lacerda Mariano L, Ingersoll MA. The immune response to infection in the bladder. *Nat Rev Urol* 2020;**17**:439–58. <https://doi.org/10.1038/s41585-020-0350-8>.
- 38 Nowroozilarki N, Öz HH, Schroth C, Hector A, Nürnberg B, Hartl D, *et al.* Anti-inflammatory role of CD11b+Ly6G+ neutrophilic cells in allergic airway inflammation in mice. *Immunol Lett* 2018;**204**:67–74. <https://doi.org/10.1016/j.imlet.2018.10.007>.
- 39 Tam JW, Kullas AL, Mena P, Bliska JB, Van der Velden AWM. CD11b+ Ly6Chi Ly6G-immature myeloid cells recruited in response to Salmonella enterica serovar typhimurium infection exhibit protective and immunosuppressive properties. *Infect Immun* 2014;**82**:2606–14. <https://doi.org/10.1128/IAI.01590-13>.
- 40 Neeli I, Khan SN, Radic M. Histone Deimination As a Response to Inflammatory Stimuli in Neutrophils. *J Immunol* 2008;**4**:.
- 41 Abraham SN, Miao Y. The nature of immune responses to urinary tract infections. *Nat Rev Immunol* 2015;**15**:655–63. <https://doi.org/10.1038/nri3887>.
- 42 Chromek M, Tullus K, Lundahl J, Brauner A. Tissue Inhibitor of Metalloproteinase 1 Activates Normal Human Granulocytes, Protects Them from Apoptosis, and Blocks Their Transmigration during Inflammation. *Infect Immun* 2004;**72**:82–8. <https://doi.org/10.1128/IAI.72.1.82-88.2004>.

- 43 Ingersoll MA, Kline KA, Nielsen H V., Hultgren SJ. G-CSF induction early in uropathogenic *Escherichia coli* infection of the urinary tract modulates host immunity. *Cell Microbiol* 2008;**10**:2568–78. <https://doi.org/10.1111/j.1462-5822.2008.01230.x>.
- 44 Lawlor KE, Campbell IK, Metcalf D, O'Donnell K, Van Nieuwenhuijze A, Roberts AW, *et al.* Critical role for granulocyte colony stimulating factor in inflammatory arthritis. *Proc Natl Acad Sci U S A* 2004;**101**:11398–403. <https://doi.org/10.1073/pnas.0404328101>.
- 45 Talhouk RS, Bissell MJ, Werb Z. Coordinated expression of extracellular matrix-degrading proteinases and their inhibitors regulates mammary epithelial function during involution. *J Cell Biol* 1992;**118**:1271–82. <https://doi.org/10.1083/jcb.118.5.1271>.
- 46 Khokha R, Werb Z. Mammary gland reprogramming: Metalloproteinases couple form with function. *Cold Spring Harb Perspect Biol* 2011;**3**:1–19. <https://doi.org/10.1101/cshperspect.a004333>.
- 47 Alexander CM, Selvarajan S, Mudgett J, Werb Z. Stromelysin-1 regulates adipogenesis during mammary gland involution. *J Cell Biol* 2001;**152**:693–703. <https://doi.org/10.1083/jcb.152.4.693>.
- 48 Schwertfeger KL, Richert MM, Anderson SM. Mammary gland involution is delayed by activated Akt in transgenic mice. *Mol Endocrinol* 2001;**15**:867–81. <https://doi.org/10.1210/mend.15.6.0663>.
- 49 Stille JAW, Birt JA, Nagel SC, Sutovsky M, Sutovsky P, Sharpe-Timms KL. Neutralizing TIMP1 restores fecundity in a rat model of endometriosis and treating control rats with TIMP1 causes anomalies in ovarian function and embryo development. *Biol Reprod* 2010;**83**:185–94. <https://doi.org/10.1095/biolreprod.109.083287>.
- 50 Lim CL, Or YZ, Ong Z, Chung HH, Hayashi H, Shrestha S, *et al.* Estrogen exacerbates mammary involution through neutrophil dependent and independent mechanism. *Elife* 2020;**9**:1–65. <https://doi.org/10.7554/eLife.57274>.
- 51 Tower H, Dall G, Davey A, Stewart M, Lanteri P, Ruppert M, *et al.* Estrogen-induced immune changes within the normal mammary gland. *Sci Rep* 2022;**12**:1–14. <https://doi.org/10.1038/s41598-022-21871-4>.
- 52 Carey AJ, Tan CK, Ipe DS, Sullivan MJ, Cripps AW, Schembri MA, *et al.* Urinary tract infection of mice to model human disease: Practicalities, implications and limitations. *Crit Rev Microbiol* 2016;**42**:780–99. <https://doi.org/10.3109/1040841X.2015.1028885>.

- 53 Fu A, Yao B, Dong T, Chen Y, Yao J, Liu Y, *et al.* Tumor-resident intracellular microbiota promotes metastatic colonization in breast cancer. *Cell* 2022;1356–72. <https://doi.org/10.1016/j.cell.2022.02.027>.
- 54 Christine M. Velicer, Susan R. Heckbert, Johanna W. Lampe, John D. Potter, Carol A. Robertson SHT. Antibiotic use in relation to the risk of breast cancer. *JAMA - J Am Med Assoc* 2004;**12**:263. <https://doi.org/10.1097/01.idc.0000130890.12611.f3>.
- 55 Hannan TJ, Mysorekar IU, Hung CS, Isaacson-Schmid ML, Hultgren SJ. Early severe inflammatory responses to uropathogenic *E. coli* predispose to chronic and recurrent urinary tract infection. *PLoS Pathog* 2010;**6**:29–30. <https://doi.org/10.1371/journal.ppat.1001042>.
- 56 Semerad CL, Liu F, Gregory AD, Stumpf K, Link DC. G-CSF is an essential regulator of neutrophil trafficking from the bone marrow to the blood. *Immunity* 2002;**17**:413–23. [https://doi.org/10.1016/S1074-7613\(02\)00424-7](https://doi.org/10.1016/S1074-7613(02)00424-7).
- 57 Fernandez M, Minguell JJ. G-CSF regulates the expression of mRNA for collagen type VI and collagen VI production in human bone marrow stromal cells. *Hematology* 1997;**2**:219–27. <https://doi.org/10.1080/10245332.1997.11746340>.
- 58 Lyons TR, O'Brien J, Borges VF, Conklin MW, Keely PJ, Eliceiri KW, *et al.* Postpartum mammary gland involution drives progression of ductal carcinoma in situ through collagen and COX-2. *Nat Med* 2011;**17**:1109–16. <https://doi.org/10.1038/nm.2416>.
- 59 Callaway MK, dos Santos CO. Gestational Breast Cancer – a Review of Outcomes, Pathophysiology, and Model Systems. *J Mammary Gland Biol Neoplasia* 2023;**28**:1–15. <https://doi.org/10.1007/s10911-023-09546-w>.
- 60 Zhang X, Abdelrahman A, Vollmar B, Zechner D. The ambivalent function of YAP in apoptosis and cancer. *Int J Mol Sci* 2018;**19**:1–21. <https://doi.org/10.3390/ijms19123770>.
- 61 Takawale A, Zhang P, Patel VB, Wang X, Oudit G, Kassiri Z. Tissue Inhibitor of Matrix Metalloproteinase-1 Promotes Myocardial Fibrosis by Mediating CD63-Integrin β 1 Interaction. *Hypertension* 2017;**69**:1092–103. <https://doi.org/10.1161/HYPERTENSIONAHA.117.09045>.
- 62 Manouryl B, Lagente V. TIMP-1 IS A KEYFACTOR OF FIBROGENIC RESPONSE TO BLEOMYCIN IN MOUSE LUNG. *Int J Immunopathol Pharmacol* 2006;**19**:471–87.
- 63 Zhang X, Chen X, Hong Q, Lin H, Zhu H, Liu Q, *et al.* TIMP-1 promotes age-related renal

- fibrosis through upregulating ICAM-1 in human TIMP-1 transgenic mice. *Journals Gerontol - Ser A Biol Sci Med Sci* 2006;**61**:1130–43. <https://doi.org/10.1093/gerona/61.11.1130>.
- 64 Chromek M, Tullus K, Hertting O, Jaremko G, Khalil A, Li YH, *et al*. Matrix metalloproteinase-9 and tissue inhibitor of metalloproteinases-1 in acute pyelonephritis and renal scarring. *Pediatr Res* 2003;**53**:698–705. <https://doi.org/10.1203/01.PDR.0000057575.86337.CB>.
- 65 Wang X, Rojas-Quintero J, Wilder J, Tesfaigzi Y, Zhang D, Owen CA. Tissue Inhibitor of Metalloproteinase-1 Promotes Polymorphonuclear Neutrophil (PMN) Pericellular Proteolysis by Anchoring Matrix Metalloproteinase-8 and -9 to PMN Surfaces. *J Immunol* 2019;**202**:3267–81. <https://doi.org/10.4049/jimmunol.1801466>.

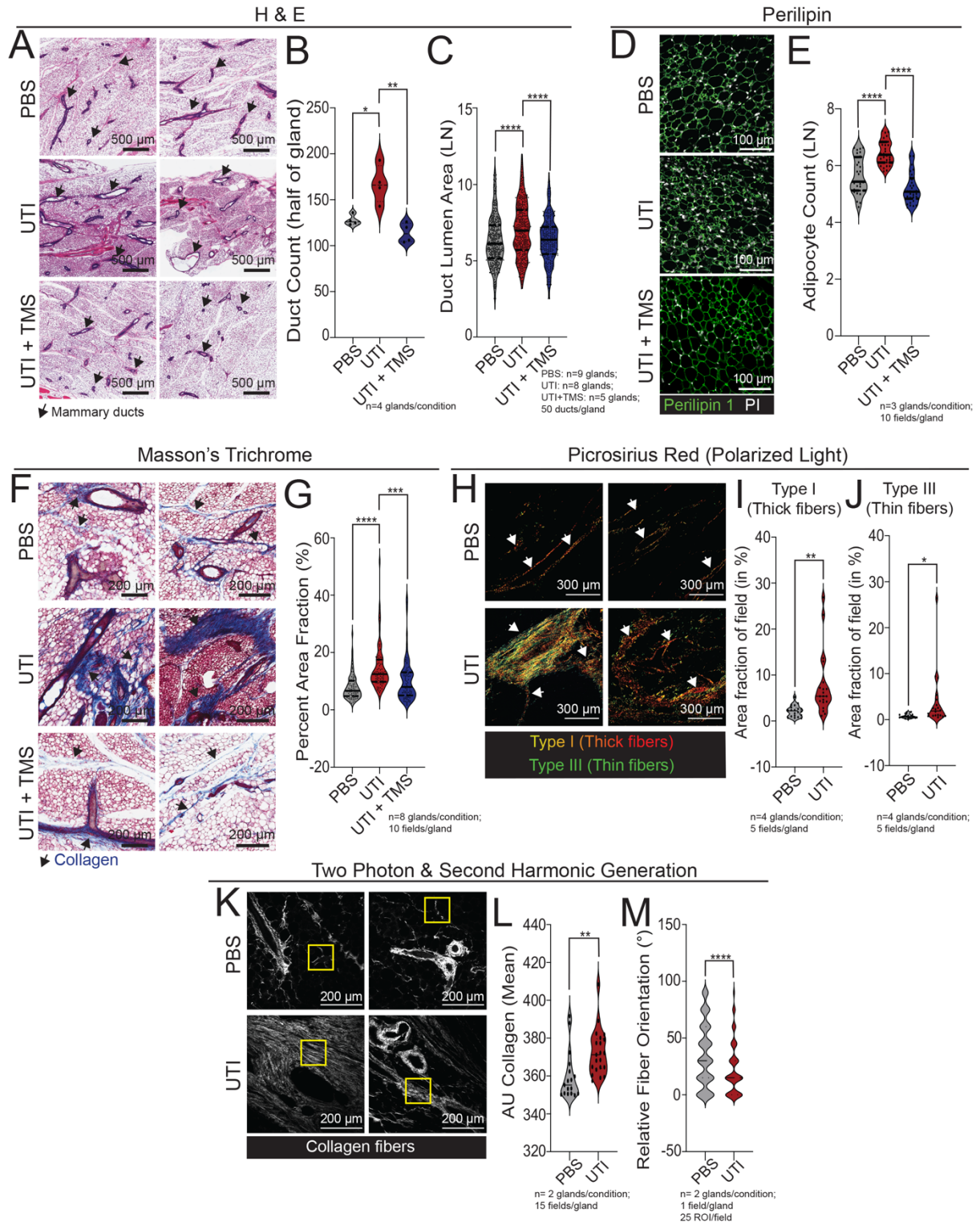


Fig. 1. UTI-bearing mice have altered mammary tissue homeostasis. (A-C) H&E staining of mammary tissue sections and **(B)** quantification of ductal counts and **(C)** quantification of ductal

lumen area in mammary tissue from PBS control mice (n=9), from UTI-bearing mice (n=8) and from UTI-bearing mice treated with TMS (n=5) at 2 weeks post-infection (p.i.). Scale bar = 500 μ m. Arrows indicate mammary ducts. Violin plots show data distribution with median (solid line) and quartiles (dashed line) indicated. * $p \leq 0.05$; ** $p \leq 0.01$; **** $p \leq 0.0001$. **(D-E)** Immunostaining of mammary tissue sections and **(E)** quantification of Perilipin+ adipocytes (green) and PI (white) from PBS control mice (n=3), from UTI-bearing mice (n=3) and from UTI-bearing mice treated with TMS (n=3) at 2 weeks post-infection (p.i.). Scale bar = 100 μ m. Violin plots show data distribution with median (solid line) and quartiles (dashed line) indicated. **** $p \leq 0.0001$. **(F-G)** Masson's trichrome staining of mammary tissue sections and **(G)** quantification of positively stained collagen (in blue) from PBS control mice (n=8), from UTI-bearing mice (n=8), and from UTI-bearing mice treated with TMS (n=8) at 2 weeks p.i.. Scale bar = 200 μ m. Arrows indicate positively stained collagen (in blue). Violin plots show data distribution with median (solid line) and quartiles (dashed line) indicated. *** $p \leq 0.001$; **** $p \leq 0.0001$. **(H-J)** Picrosirius red staining in mammary tissue sections, and quantification of **(I)** type I collagen (thick fibers) and **(J)** type III collagen (thin fibers), from PBS control mice (n=4), and from UTI-bearing mice (n=4), at 2 weeks p.i.. Stained slides were imaged under linearly polarized light. Scale bar = 300 μ m. Arrows indicate collagen fibers. Violin plots show data distribution with median (solid line) and quartiles (dashed line) indicated. * $p \leq 0.05$; ** $p \leq 0.01$. **(K-M)** Two-photon & second harmonic generation imaging of H&E stained mammary gland slides, and quantification of **(L)** total collagen signal, and **(M)** collagen orientation, from PBS control mice (n=2), and from UTI-bearing mice (n=2), at 2 weeks p.i.. Stained slides were imaged under linearly polarized light. Scale bar = 200 μ m. Yellow boxes indicate collagen fibers. Violin plots show data distribution with median (solid line) and quartiles (dashed line) indicated. ** $p \leq 0.01$; *** $p \leq 0.001$.

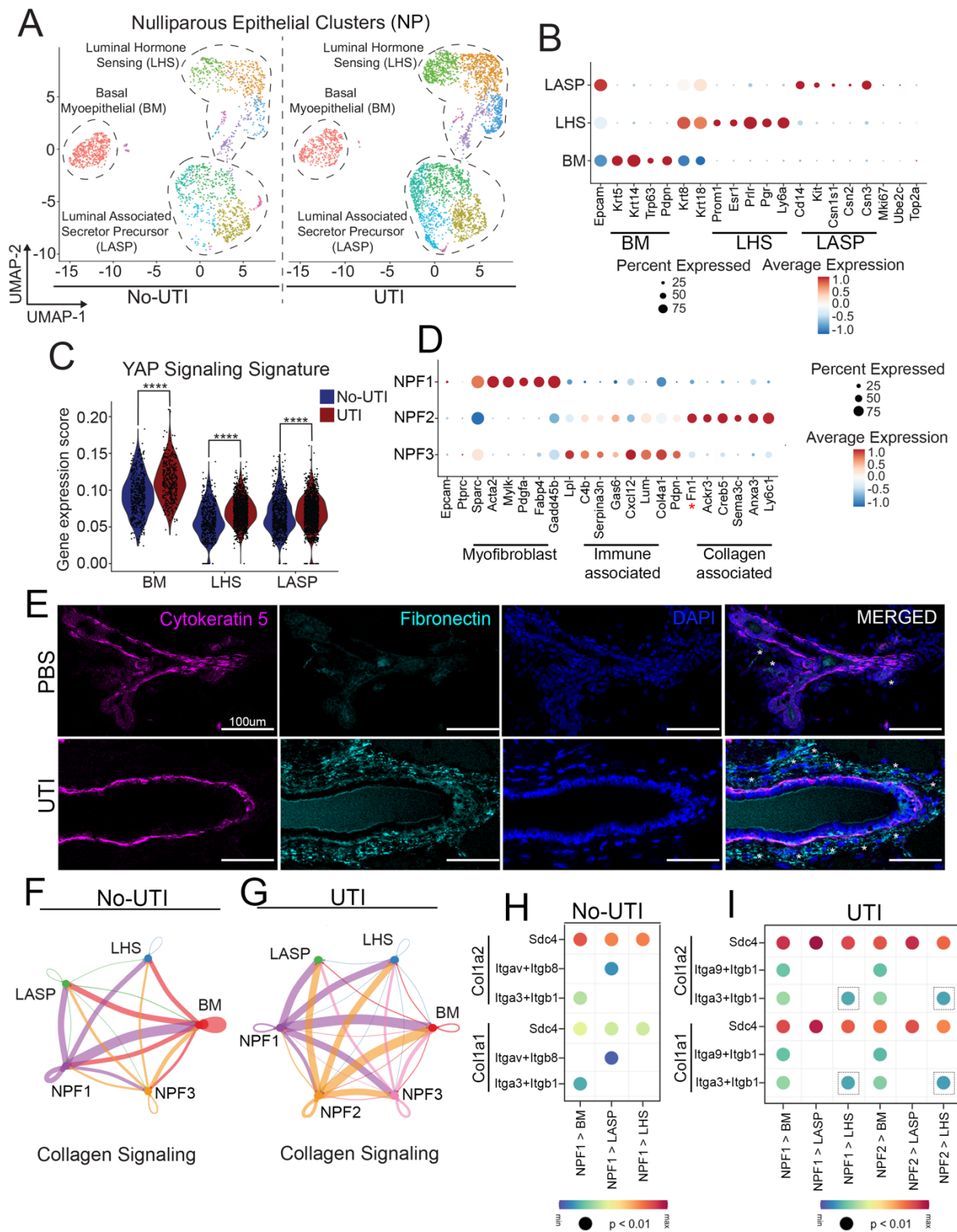


Fig. 2. scRNA-seq analysis identifies mammary molecular and cellular alterations induced by the onset of UTI. (A-B) UMAP and **(B)** lineage classification of mammary epithelial cells from uninfected mice (No-UTI) and UTI-bearing mice (UTI, 2 weeks post-infection (p.i.)). **(C)** Violin plot showing gene expression score of YAP Signaling signature across major epithelial lineages from uninfected mice (No-UTI, blue) and UTI-bearing mice (red). **** $p \leq 0.0001$. **(D)** Dotplot showing average expression of genes associated with myofibroblast state, immuno-related fibroblast state, or collagen-Fn1-related fibroblast. **(E)** Immunostaining analysis showing Cytokeratin 5+ MECs (magenta), DAPI (blue), and Fibronectin (Fn1)+ fibroblasts (cyan) in mammary tissue from PBS control and UTI-bearing mice, at 2 weeks p.i.. Scale bar = 200 μ m. White asterix (*) indicate Fn1+ fibroblasts. **(F-G)** Intensity plot showing Collagen signaling cell-cell interactions in fibroblasts from **(F)** uninfected mice (No-UTI) and **(G)** UTI-bearing mice (UTI). **(H-I)**. Top significant ligand-receptor pairs associated with Collagen signaling in **(H)** uninfected mice (No-UTI) and **(I)** UTI-bearing mice (UTI). Dashed squares indicate gains of pairs in LHS cells from UTI-bearing mice, at 2 weeks p.i.

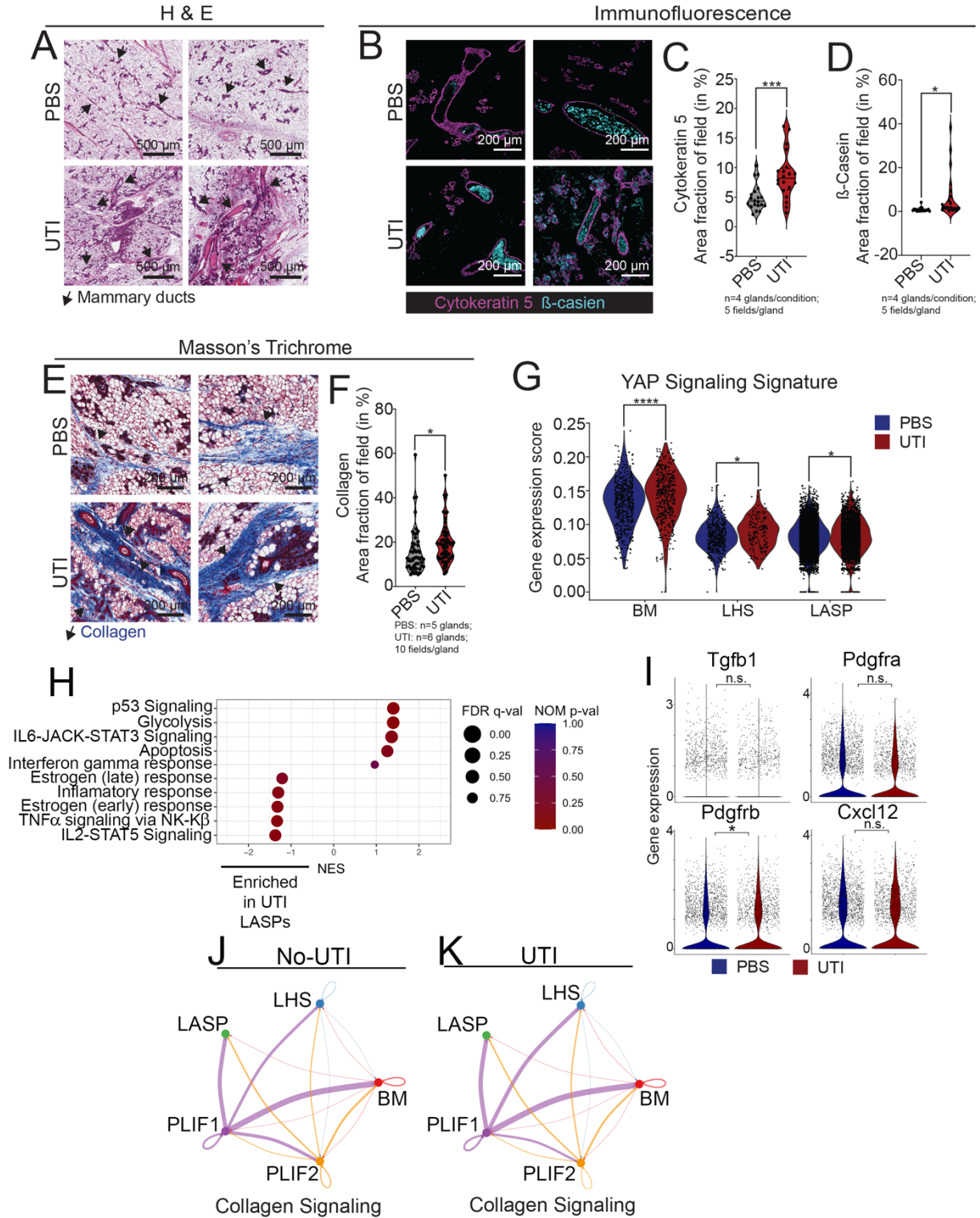


Fig. 3. The onset of UTI alters mammary gland post-lactation involution (PLI). (A) H&E staining of mammary tissue sections from PLI PBS control mice and PLI UTI-bearing mice, at 2 weeks post-infection (p.i.). Arrows indicate mammary ducts. (B-D) Immunostaining analysis showing Cytokeratin 5+ MECs (magenta) and β -casein (cyan), and quantification of (C) duct structures (inferred by Cytokeratin 5 signal), and (D) β -casein levels in the mammary tissue from PLI PBS control mice (n=4) and PLI UTI-bearing mice (n=4), at 2 weeks p.i.. Scale bar = 200 μ m. Violin plots show data distribution with median (solid line) and quartiles (dashed line) indicated. * $p \leq 0.05$; *** $p \leq 0.001$. (E-F) Masson's trichrome staining of mammary tissue sections and (F) quantification of positively stained collagen (in blue) from PLI PBS control mice (n=5) and PLI UTI-bearing mice (n=6), at 2 weeks p.i.. Scale bar = 200 μ m. Arrows indicate positively stained collagen (in blue). Violin plots show data distribution with median (solid line) and quartiles (dashed line) indicated. * $p \leq 0.05$. (G) Violin plot showing gene expression score of YAP Signaling signature across major epithelial lineages from PLI PBS control mice (blue) and PLI UTI-bearing mice (red), at 2 weeks p.i.. * $p \leq 0.05$; **** $p \leq 0.0001$. (H) Gene-set enrichment analysis (GSEA) of LSPs cells from PLI PBS control mice (positive NES) and PLI UTI-bearing mice (negative NES), at 2 weeks p.i.. Plot displays the top 5 pathways for each condition. (I) Violin plots showing gene expression levels of involution-induced, activated fibroblasts. (J-K) Intensity plot showing Collagen signaling cell-cell interactions in fibroblasts from (J) PLI PBS control mice and (K) PLI UTI-bearing mice at 2 weeks p.i..

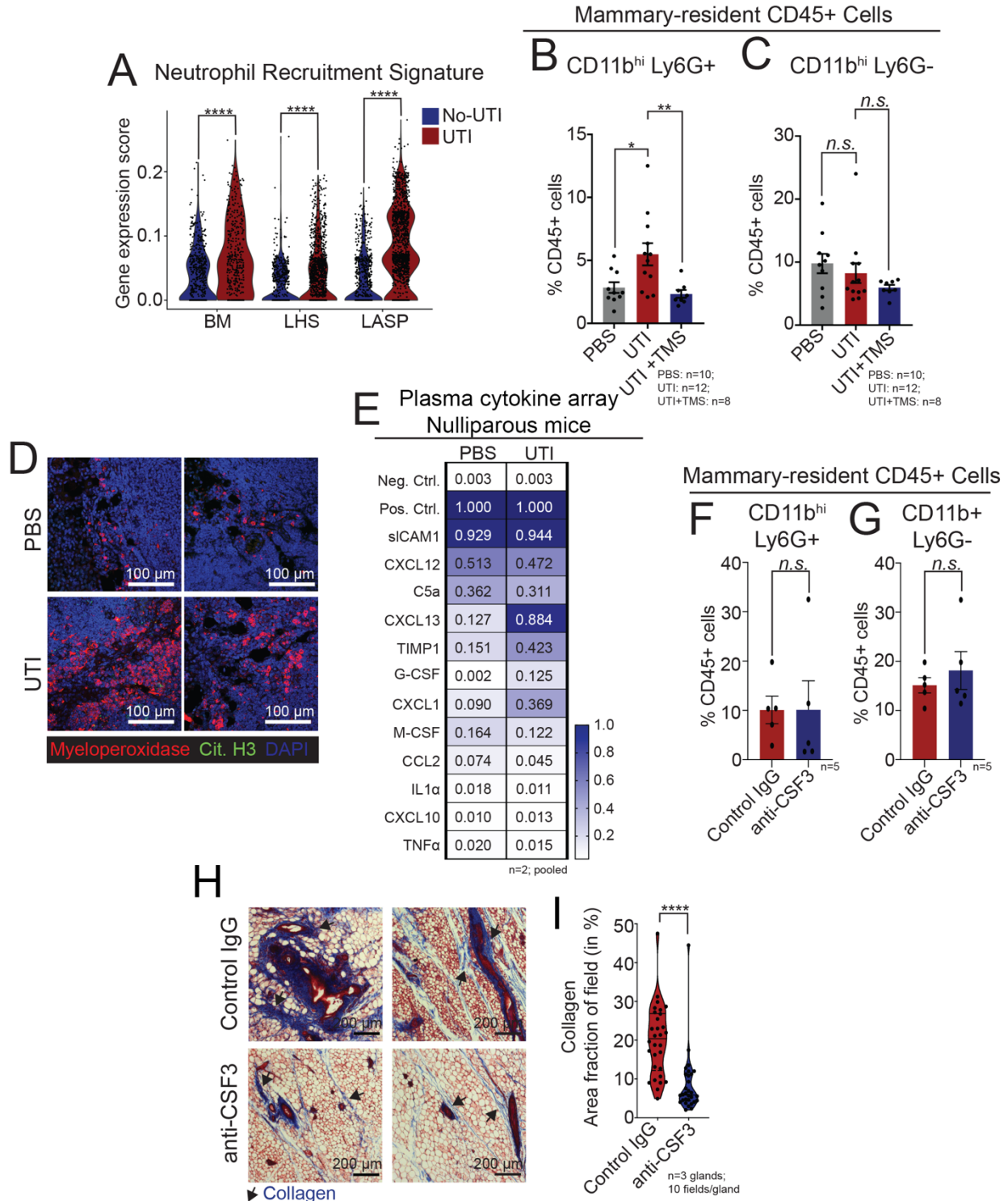


Fig. 4. UTI-bearing mice have altered mammary neutrophil infiltration and elevated G-CSF in circulating plasma. (A) Violin plot showing gene expression score of Neutrophil Recruitment

signature across major epithelial lineages from nulliparous (NP) PBS control mice (blue) and NP UTI-bearing mice (red). **** $p \leq 0.0001$. **(B-C)** Flow cytometry quantification of mammary-resident **(B)** CD11b^{hi}Ly6G⁺ neutrophils, and **(C)** CD11b+Ly6G⁻ (myeloid) cells from NP PBS mice (n=10), from NP UTI-bearing mice (n=12), and from NP UTI-bearing mice treated with TMS (n=8) at 2 weeks post-infection (p.i.). Error bars represent mean \pm S.E.M. * $p \leq 0.05$; ** $p \leq 0.01$. **(D)** Immunostaining analysis of Myeloperoxidase⁺ neutrophils (Mpo⁺, red) and Citrullinated histone H3⁺ neutrophils (Cit. H3., in green) in mammary tissue sections from NP PBS control mice and NP UTI-bearing mice, at 2 weeks p.i.. Scale bar = 100 μ m. **(E)** Cytokine quantification of plasma collected from NP PBS control mice (n=2 samples pooled) and NP UTI-bearing mice (n=2 samples pooled) at 2 weeks p.i.. **(F-G)** Flow cytometry quantification of mammary-resident **(F)** CD11b^{hi}Ly6G⁺ neutrophils, and **(G)** CD11b+Ly6G⁻ (myeloid) cells from NP UTI-bearing mice after 6 doses of IgG control (n=5) or anti-CSF3 neutralizing antibody (n=5). Error bars represent mean \pm S.E.M. **(H-I)** Masson's trichrome staining of mammary tissue sections and **(I)** quantification of positively stained collagen (in blue) from NP UTI-bearing mice after 6 doses of IgG control (n=3) or anti-CSF3 neutralizing antibody (n=3). Scale bar = 200 μ m. Arrows indicate positively stained collagen (in blue). Violin plots show data distribution with median (solid line) and quartiles (dashed line) indicated. **** $p \leq 0.0001$.

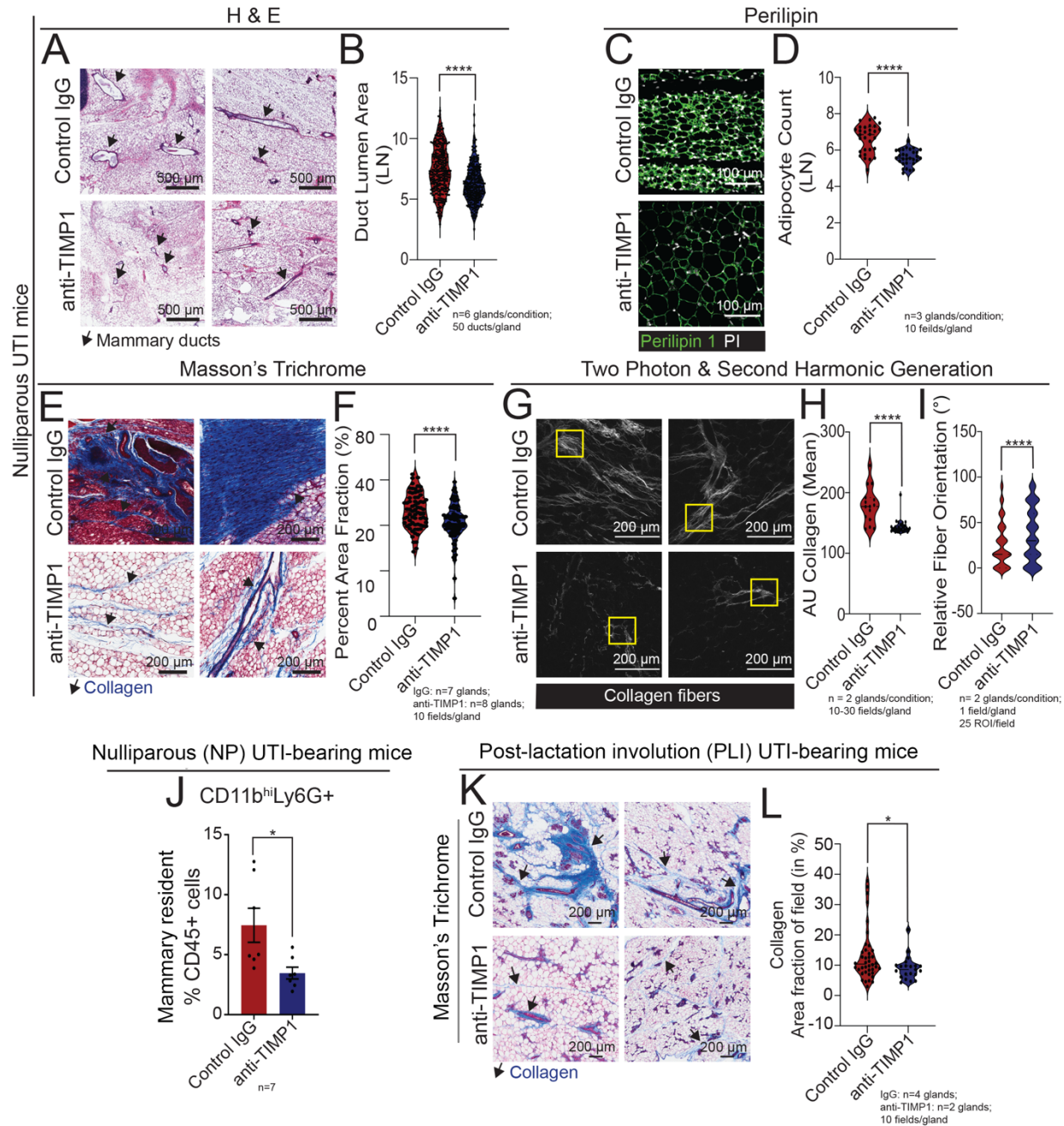


Fig. 5. Neutralization of TIMP1 normalizes mammary duct abnormality, ECM content, and neutrophil infiltration in nulliparous UTI-bearing mice. (A-B) H&E staining of mammary tissue sections and **(B)** quantification of ductal lumen area in mammary tissue from nulliparous (NP) UTI-bearing mice after 6 doses of IgG control (n=6) and anti-TIMP1 neutralizing antibody (n=6). Scale bar = 500 μ m. Arrows indicate mammary ducts. Violin plots show data distribution with median (solid line) and quartiles (dashed line) indicated. ****p<0.0001. **(C-D)** Immunostaining of mammary tissue sections and **(D)** quantification of Perilipin+ adipocytes (green), and PI (white),

from NP UTI-bearing mice after 6 doses of IgG control (n=3) and anti-TIMP1 neutralizing antibody (n=3). Scale bar = 100 μ m. Violin plots show data distribution with median (solid line) and quartiles (dashed line) indicated. **** $p \leq 0.0001$. **(E-F)** Masson's trichrome staining of mammary tissue sections and **(F)** quantification of positively stained collagen (in blue) from NP UTI-bearing mice after 6 doses of IgG control (n=7) or anti-TIMP1 neutralizing antibody (n=8). Scale bar = 200 μ m. Arrows indicate positively stained collagen (in blue). Violin plots show data distribution with median (solid line) and quartiles (dashed line) indicated. **** $p \leq 0.0001$. **(G-I)** Two-photon & second harmonic generation imaging of H&E stained mammary gland slides, and quantification of **(H)** total collagen signal, and **(I)** collagen orientation from NP UTI-bearing mice after 6 doses of IgG control (n=2) or anti-TIMP1 neutralizing antibody (n=2). Scale bar = 200 μ m. Arrows indicate positively stained collagen (in blue). Violin plots show data distribution with median (solid line) and quartiles (dashed line) indicated. **** $p \leq 0.0001$. **(J)** Flow cytometry quantification of mammary-resident CD11b^{hi}Ly6G⁺ neutrophils from NP UTI-bearing mice after 6 doses of IgG control (n=7) or anti-TIMP1 neutralizing antibody (n=7). Error bars represent mean \pm S.E.M. * $p \leq 0.05$. **(K-L)** Masson's trichrome staining of mammary tissue sections and **(L)** quantification of positively stained collagen (in blue) from post-lactation involution (PLI) UTI-bearing mice after 6 doses of IgG control (n=4) or anti-TIMP1 neutralizing antibody (n=2). Scale bar = 200 μ m. Arrows indicate positively stained collagen (in blue). Violin plots show data distribution with median (solid line) and quartiles (dashed line) indicated. * $p \leq 0.05$.

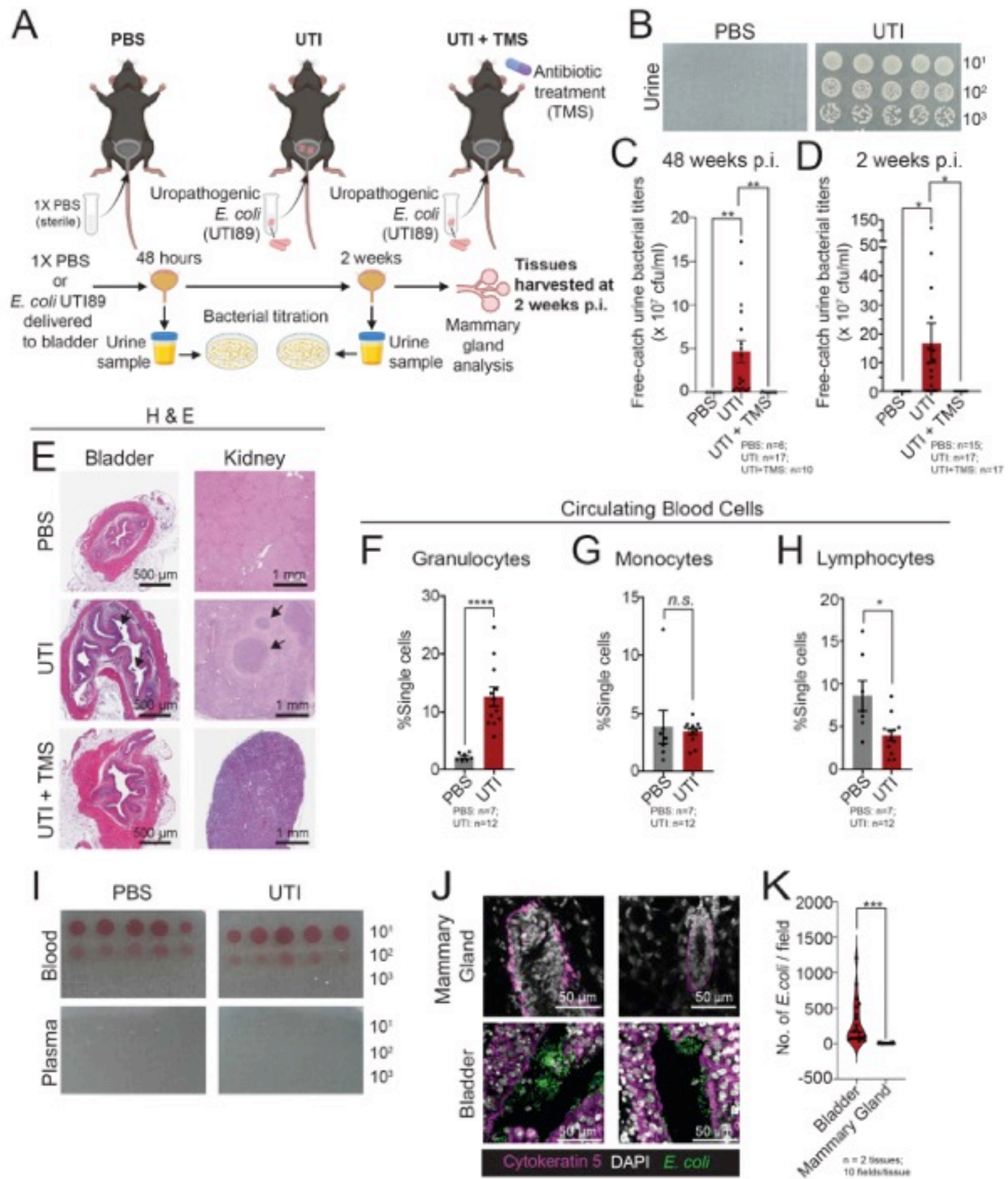


Fig. S1. UPEC infection in nulliparous C57BL/6 mice. **(A)** Experimental design showing nulliparous administered with either 1X PBS (PBS), uropathogenic *E. coli* strain UTI89 (UTI) transurethrally. A subset of *E. coli* infected mice were also treated with antibiotic TMS treatment (UTI+TMS). Bacterial titers of free-catch urine samples were conducted at 48 hours and 2 weeks post-infection (p.i.). Tissues were assessed at 2 weeks p.i. Created with BioRender.com. **(B)** Example of LB agar spot cultures of urine obtained from PBS control mice, or UTI-bearing mice. Diluted 10-fold from 10^{-1} to 10^{-3} in sterile 1X PBS. **(C-D)** Bacterial titers of free-catch urine samples, collected at **(C)** 48 hours and **(D)** 2 weeks post-infection (p.i.) from PBS control mice, UTI-bearing mice, and from UTI-bearing mice treated with TMS. Error bars represent mean \pm S.E.M. * $p \leq 0.05$; ** $p \leq 0.01$. **(E)** H&E-staining in histological sections of bladder and kidney tissues from PBS control mice and UTI-bearing mice. Scale bar = 500 μ m and 1 mm, respectively. Arrows indicate signs of urothelial erosion and immune infiltration as confirmed by pathological analysis. **(F-H)** Flow cytometry quantification at 2 weeks p.i. of **(F)** granulocytes, **(G)** monocytes and **(H)** lymphocytes in blood collected from PBS control mice (n=7) and UTI-bearing mice (n=12). Error bars represent mean \pm S.E.M. * $p \leq 0.05$, **** $p \leq 0.0001$. **(I)** LB agar spot cultures of blood and plasma collected from PBS control mice and UTI-bearing mice at 2 weeks p.i. Diluted 10-fold from 10^{-1} to 10^{-3} in sterile 1X PBS. **(J-K)** Immunofluorescence staining of cytokeratin 5 (magenta), DAPI (white) and *E. coli* (green) in mammary gland and bladder tissue sections from UTI-bearing mice. Scale bar = 50 μ m. n=2 tissues. **(H)** *E. coli* staining quantification in mammary gland and bladder tissue sections from UTI-bearing mice. *E. coli* counted for 10 fields per tissue section. Violin plots show data distribution with median (solid line) and quartiles (dashed line) indicated. *** $p \leq 0.001$

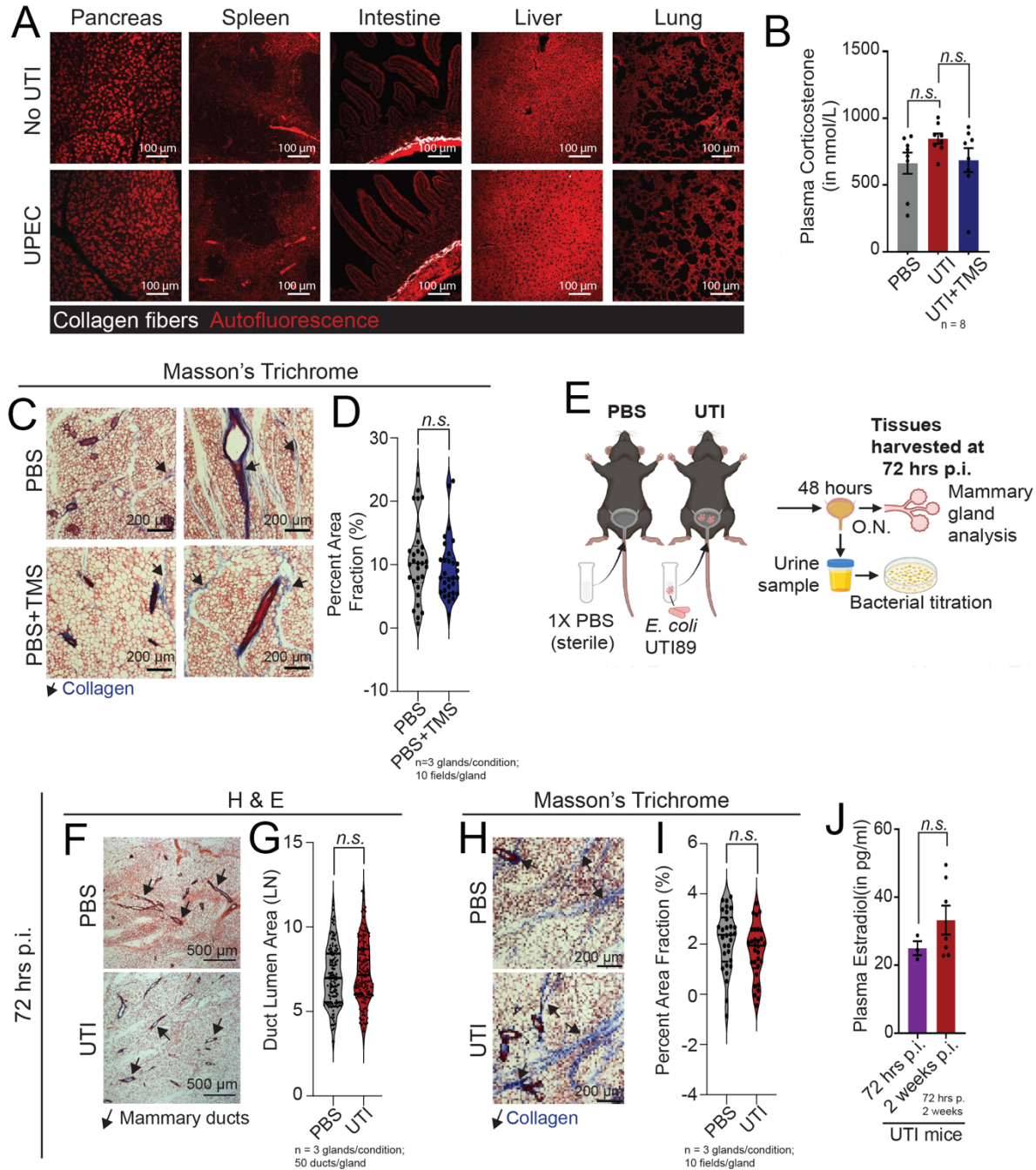


Fig. S2. Characterization of ECM alterations in nulliparous UTI-bearing mice. (A) Two photon microscopy and second harmonic generation images of H&E-stained tissue sections from pancreas, spleen, intestine, liver and lungs of PBS control mice and UTI-bearing mice, showing collagen fibers (white) and tissue auto-fluorescence (red). Scale bar = 100 μ m. **(B)** Elisa

quantification of plasma corticosterone levels in PBS control mice (n=8), UTI-bearing mice (n=8), and UTI-bearing mice treated with TMS (n=8) at 2 weeks post infection (p.i.). Error bars represent mean \pm S.E.M. **(C-D)** Masson Trichrome blue staining of mammary tissue sections and **(D)** quantification of positively stained collagen (in blue) from PBS control mice (n=3), PBS control mice treated with TMS (2 weeks of treatment, n=3). Scale bar = 200 μ m. Arrows indicate positively stained collagen (in blue). Violin plots show data distribution with median (solid line) and quartiles (dashed line) indicated. **(E)** Experimental design showing nulliparous mice administered 1X PBS (PBS) or uropathogenic *E. coli* strain UTI89 (UTI). Bacterial titers of free-catch urine samples were conducted at 48 hours p.i. and tissues were assessed at 72 hours p.i. Created with BioRender.com. **(F-G)** H&E staining of mammary tissue sections and **(G)** quantification of ductal lumen area of mammary tissue sections from PBS control mice (n=3) and UTI-bearing mice (n=3) at 72 hours p.i. Scale bar = 500 μ m. Arrows indicate mammary ducts. Area measured for 50 ducts/gland. Violin plots show data distribution with median (solid line) and quartiles (dashed line) indicated. **(H-I)** Masson's trichrome staining of mammary tissue sections and **(I)** quantification of positively stained collagen (blue) from PBS control mice (n=3) and UTI-bearing mice (n=3), at 72 hours p.i. Scale bar = 200 μ m. Arrows indicate areas of positively stained collagen (in blue). Area measured for 10 fields/gland. Violin plots show data distribution with median (solid line) and quartiles (dashed line) indicated. **(J)** Elisa quantification of plasma estradiol levels in UTI-bearing mice at 72 hours (n=3), and 2 weeks (n=7) p.i. Error bars represent mean \pm S.E.M.

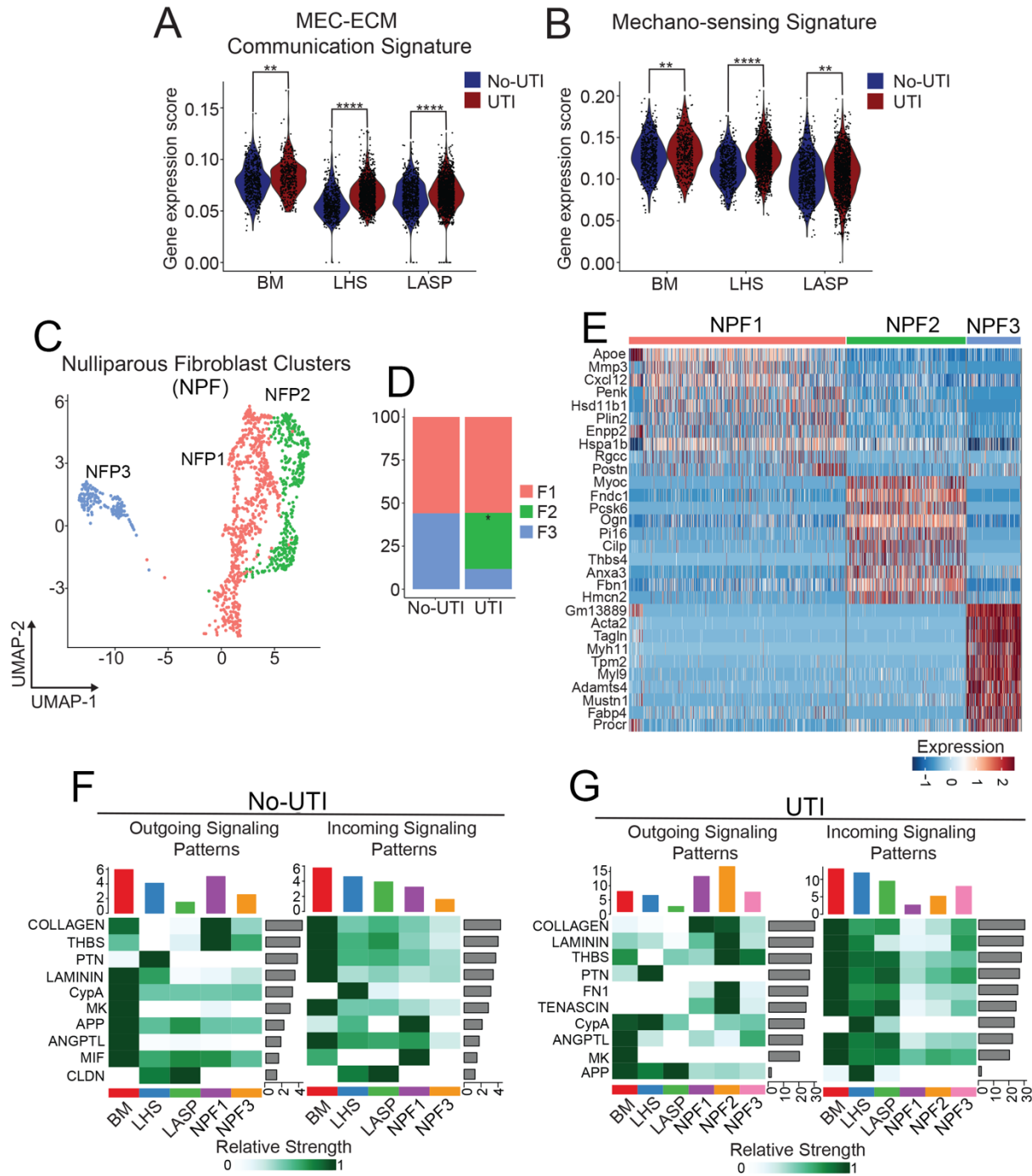


Fig. S3. scRNA-seq analysis of mammary tissue from uninfected and UTI-bearing mice. (A-B) Violin plot showing gene expression scores of **(A)** MEC-ECM Communication signatures and **(B)** Mechano-sensing signatures, in MECs from uninfected mice (No-UTI, blue) and UTI-bearing mice (red). ****** $p \leq 0.01$; ******** $p \leq 0.0001$. **(C-D)** Fibroblast **(C)** UMAP clustering and **(D)** abundance

quantification in mammary tissue of uninfected mice (No-UTI) and UTI-bearing mice. * $p \leq 0.05$.
(E) Heatmap showing top 10 differentially expressed genes across populations of mammary fibroblasts. (F-G) CellChat heatmaps showing pathways inferred to be enriched either as outgoing or incoming signaling patterns in MECs (BM, LHS, LASP) or fibroblasts (NF1, NF2, NF3) from uninfected mice (No-UTI) and UTI-bearing mice. Colored bar plots indicate communication signal intensity. Gray side bar plots indicate enrichment for specific signaling pathways.

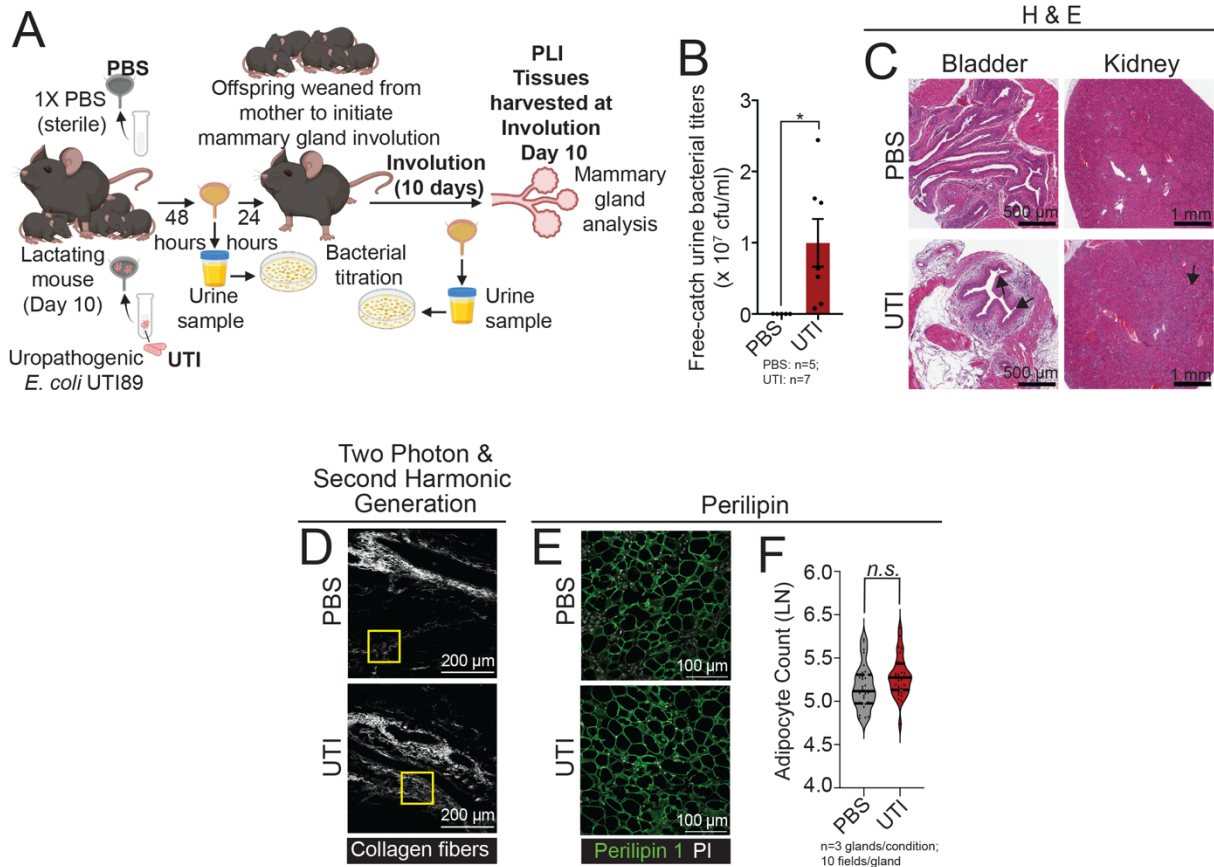


Fig. S4. UTI infection of post-lactation involuting female mice. (A) Experimental design showing the utilization of post-lactation involuting female mice (PLI). On lactation day 10, the mice were administered 1X PBS (PBS) or uropathogenic *E. coli* strain UTI89 (UTI) transurethrally. Urine bacterial titers were conducted at 48 hours p.i. and pups were weaned the following day to allow for forced mammary gland involution. Urine bacterial titers and tissue analyses were conducted at forced involution day 10. Created with BioRender.com. (B) Bacterial titers of free-catch urine samples from PBS control PLI mice (n=5) and UTI-bearing PLI mice (n=7). Error bars represent mean \pm S.E.M. * $p \leq 0.05$. (C) H&E-staining in histological sections of bladder and kidney tissues from PBS control and UTI-bearing PLI mice. Scale bar = 500 μ m and 1 mm, respectively. Arrows indicate signs of urothelial erosion and immune infiltration as confirmed by pathological analysis. (D) Two photon microscopy and second harmonic generation of H&E-stained mammary tissue sections from PBS control and UTI-bearing PLI mice. Yellow square indicates areas with positive collagen signal (white). (E-F) Immunostaining of mammary tissue sections and (F) quantification of Perilipin+ adipocytes (green), PI (white), in PBS control (n=3) and UTI-bearing PLI mice (n=3). Scale bar = 100 μ m. Violin plots show data distribution with median (solid line) and quartiles (dashed line) indicated.

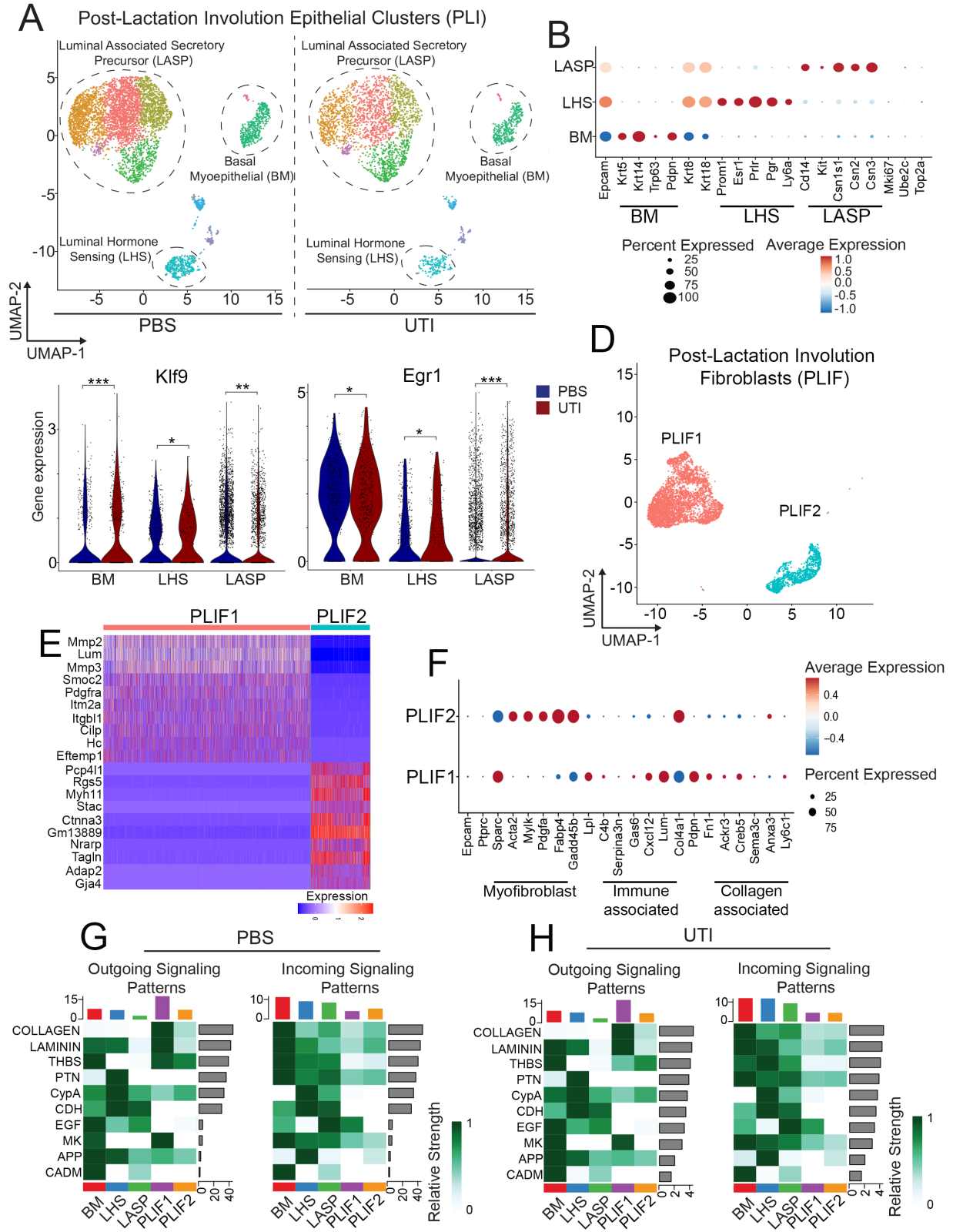


Fig. S5. scRNA-seq analysis of mammary tissue from control and UTI-bearing PLI mice. (A-B) UMAP and (B) lineage classification of mammary epithelial cells from PBS control and UTI-bearing PLI mice. (C) Violin plot showing *Egr1* and *Klf9* mRNA levels across MEC lineages from control and UTI-bearing PLI mice (D) Fibroblast UMAP clustering. (E) Heatmap showing top 10 differentially expressed genes across populations of mammary fibroblasts. (F) Dot plot showing average expression of genes of myofibroblast state, and those of Immune-associated and collagen-associated fibroblasts. (G-H) CellChat heatmaps showing pathways inferred to be enriched either as outgoing or incoming signaling patterns in MECs (BM, LHS, LASP) or fibroblasts (PLIF1, PLIF2) PBS control and UTI-bearing PLI mice. Colored bar plots indicate communication signal intensity. Gray side bar plots indicate enrichment for specific signaling pathways.

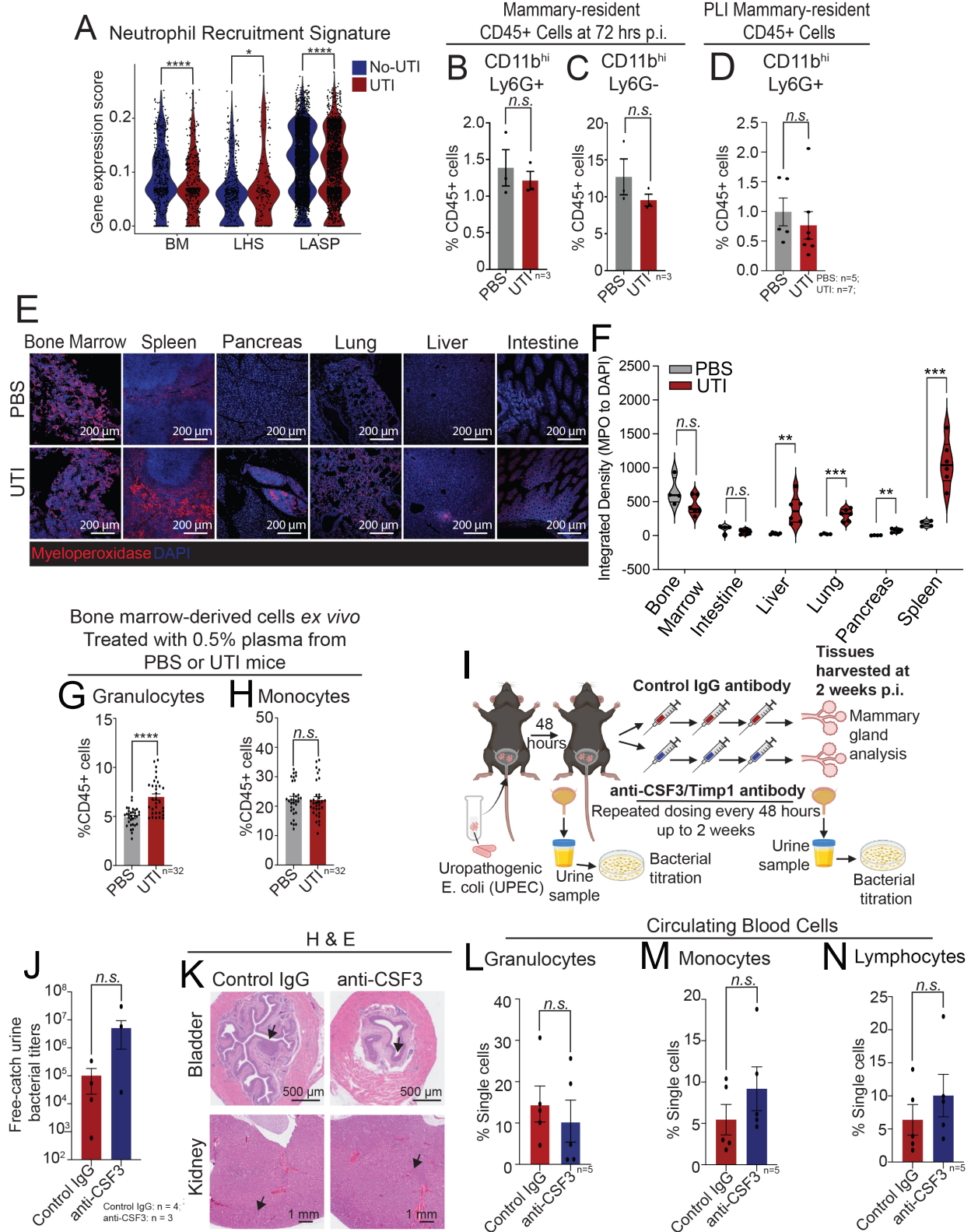


Fig. S6. Mammary immune alterations in UTI-bearing mice. **(A)** Violin plot showing gene expression scores of Neutrophil recruitment signature in MECs from uninfected mice (No-UTI) and UTI-bearing mice. * $p \leq 0.05$; **** $p \leq 0.0001$. **(B-C)** Flow cytometry analysis of neutrophil populations in the mammary tissue of nulliparous PBS control mice (n=3) and UTI-bearing mice (n=3) 72 hours p.i. Error bars represent mean \pm S.E.M. **(D)** Flow cytometry analysis of neutrophil CD11b⁺Ly6G⁺ cells in the mammary tissue of PBS control mice (n=5) and UTI-bearing mice (n=7) PLI mice, 2 weeks p.i. Error bars represent mean \pm S.E.M. **(E-F)** Immunostaining of mammary tissue sections and **(F)** quantification of Myeloperoxidase⁺ neutrophils (Mpo⁺, red) in the bone marrow, spleen, pancreas, lung, liver and intestine of nulliparous PBS control mice and UTI-bearing mice, 2 weeks p.i. Scale bar = 200 μ m. Violin plots show data distribution with median (solid line) and quartiles (dashed line) indicated. ** $p \leq 0.01$; *** $p \leq 0.001$. **(G-H)** Flow cytometry analysis of **(G)** granulocytes and **(H)** monocytes in *ex vivo* cultured bone marrow cells after treatment with 0.5% (v/v) plasma from PBS control mice (n=8) or UTI-bearing mice (n=8) for 24 hours. n=32/condition. Error bars represent mean \pm S.E.M. **(I)** Experimental design showing approach to treat UTI-bearing mice with IgG control or anti-CSF-3 neutralizing antibody (2 weeks, 6 doses). Urine bacterial titers were conducted at 48 hours p.i. Urine bacterial titers and tissue analyses were conducted 24 hours after the last treatment dose. Created with BioRender.com. **(J)** Bacterial titers of free-catch urine samples from IgG treated (n=4) or anti-CSF-3 neutralizing antibody treated (n=3) UTI-bearing mice. Error bars represent mean \pm S.E.M. **(K)** H&E-staining in histological sections of bladder and kidney tissues from IgG treated or anti-CSF-3 neutralizing antibody treated, UTI-bearing mice. Scale bar = 500 μ m and 1 mm, respectively. Arrows indicate signs of urothelial erosion and immune infiltration as confirmed by pathological analysis. **(L-N)** Flow cytometry quantification of **(L)** granulocytes, **(M)** monocytes and **(N)** lymphocytes in blood collected from IgG treated (n=5) or anti-CSF-3 neutralizing antibody treated (n=5), UTI-bearing mice. Error bars represent mean \pm S.E.M.

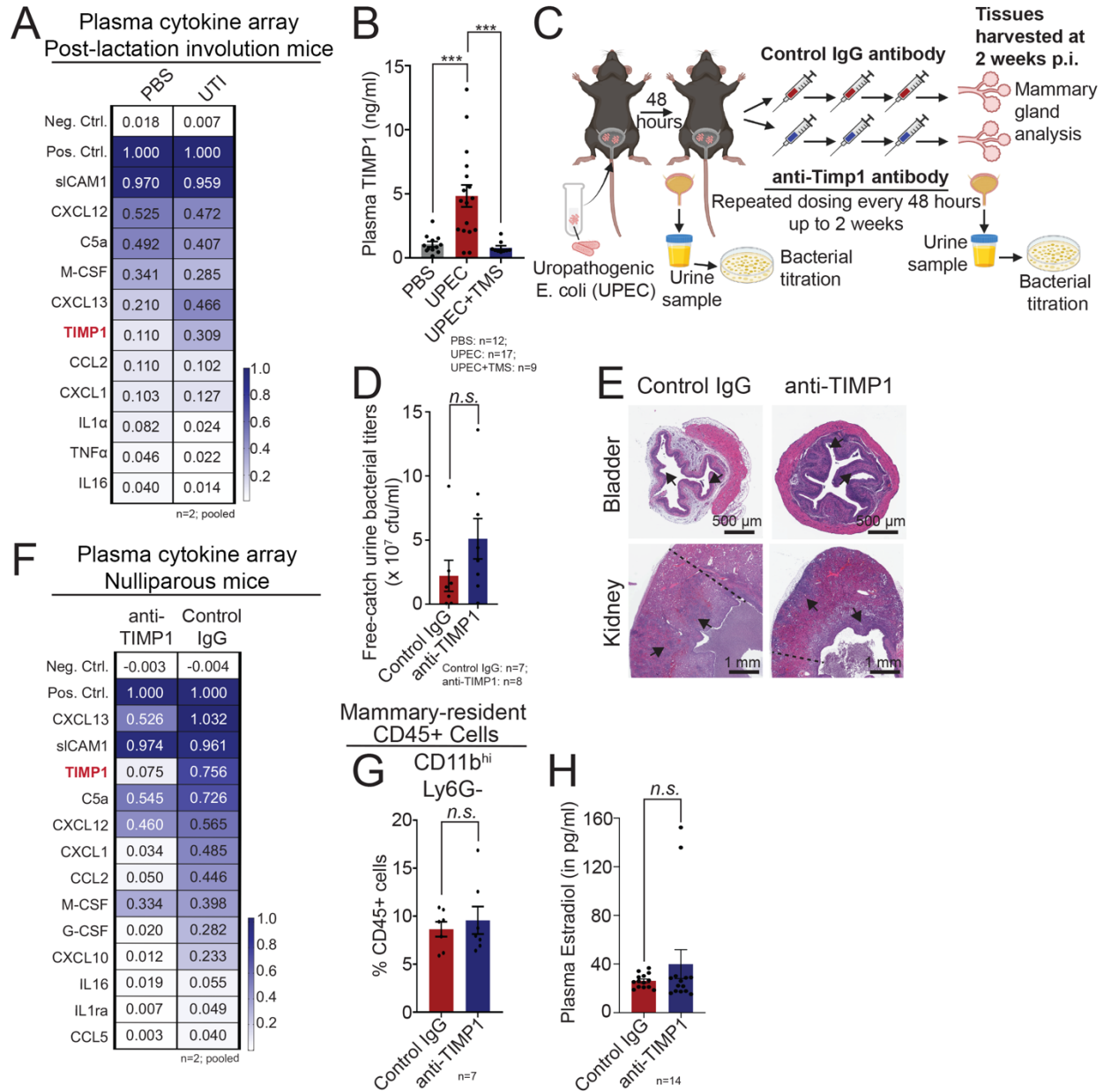


Fig. S7. Treatment of nulliparous UTI-bearing mice with TIMP1 neutralizing antibodies. (A) Cytokine analysis of plasma from PBS control and UTI-bearing post-lactation involution (PLI) mice. **(B)** Elisa quantification of plasma TIMP1 levels in PBS control mice (n=12), UTI-bearing mice (n=17), and UTI-bearing mice treated with TMS (n=9). Error bars represent mean \pm S.E.M. *** $p \leq 0.001$. **(C)** Experimental design showing approach to treat UTI-bearing mice with IgG control or anti-TIMP1 neutralizing antibody (2 weeks, 6 doses). Urine bacterial titers were conducted at 48 hours p.i. Urine bacterial titers and tissue analyses were conducted 24 hours after the last treatment. Created with BioRender.com. **(D)** Bacterial titers of free-catch urine samples from IgG

treated (n=7) or anti-TIMP1 neutralizing antibody treated (n=8) UTI-bearing mice. Error bars represent mean \pm S.E.M. **(E)** H&E-staining in histological sections of bladder and kidney tissues from IgG treated or anti-TIMP1 neutralizing antibody treated, UTI-bearing mice. Scale bar = 500 μ m and 1 mm, respectively. Arrows indicate signs of urothelial erosion and immune infiltration as confirmed by pathological analysis. **(F)** Cytokine analysis of plasma from IgG treated or anti-TIMP1 neutralizing antibody treated UTI-bearing nulliparous mice. **(G)** Flow cytometry analysis of CD11b+Ly6G⁻ mammary myeloid cells from IgG treated or anti-TIMP1 neutralizing antibody treated, UTI-bearing mice. Error bars represent mean \pm S.E.M. **(H)** Elisa (ELISA) quantification of plasma estradiol levels in IgG treated (n=14) or anti-TIMP1 neutralizing antibody treated (n=14) UTI-bearing nulliparous mice. Error bars represent mean \pm S.E.M.

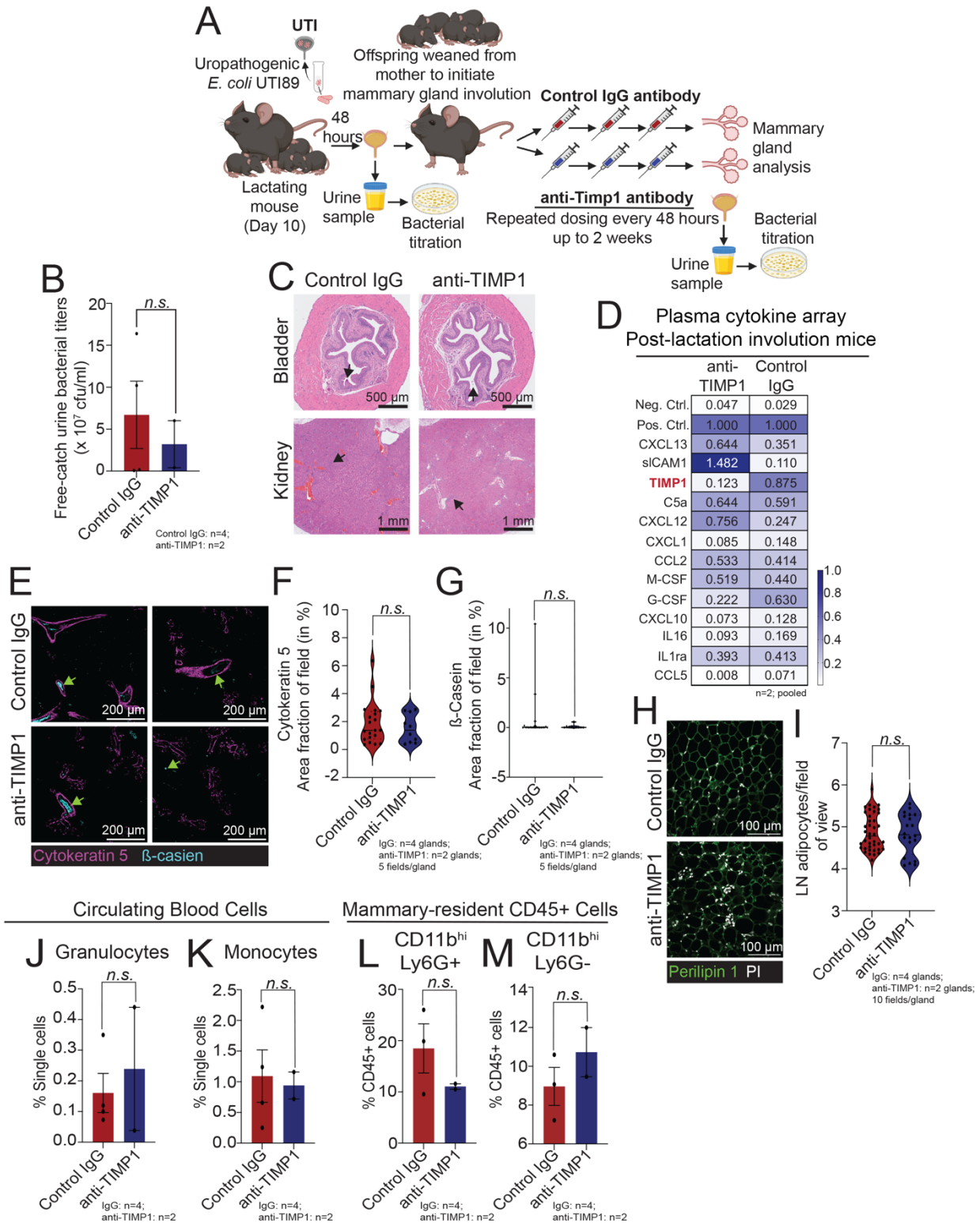


Fig. S8. Treatment of post-lactating involuting (PLI) UTI-bearing mice with TIMP1 neutralizing antibodies. (A) Experimental design showing approach to treat UTI-bearing PLI

mice with IgG control or anti-TIMP1 neutralizing antibody (2 weeks, 6 doses). Urine bacterial titers were conducted at 48 hours p.i. Urine bacterial titers and tissue analyses were conducted 24 hours after the last treatment. Created with BioRender.com. **(B)** Bacterial titers of free-catch urine samples from IgG treated (n=4) or anti-TIMP1 neutralizing antibody treated (n=2) UTI-bearing mice. Error bars represent mean \pm S.E.M. **(C)** H&E-staining in histological sections of bladder and kidney tissues from IgG treated or anti-TIMP1 neutralizing antibody treated, UTI-bearing mice. Scale bar = 500 μ m and 1 mm, respectively. Arrows indicate signs of urothelial erosion and immune infiltration as confirmed by pathological analysis. **(D)** Cytokine analysis of plasma from IgG treated or anti-TIMP1 neutralizing antibody treated UTI-bearing PLI mice. **(E-G)** Immunostaining of mammary tissue sections and **(F)** quantification of Cytokeratin 5 (magenta) and **(G)** β -casein levels (cyan) from UTI-bearing PLI mice after 6 doses of IgG control (n=4) or anti-TIMP1 neutralizing antibody (n=2). Scale bar = 200 μ m. Violin plots show data distribution with median (solid line) and quartiles (dashed line) indicated. **(H-I)** Immunostaining of mammary tissue sections and **(I)** quantification of Perilipin+ adipocytes (green) UTI-bearing PLI mice mice after 6 doses of IgG control (n=4) or anti-TIMP1 neutralizing antibody (n=2). Scale bar = 100 μ m. Violin plots show data distribution with median (solid line) and quartiles (dashed line) indicated. **(J-K)** Flow cytometry analysis of circulating **(J)** granulocytes and **(K)** monocytes from IgG treated (n=4) or anti-TIMP1 neutralizing antibody treated (n=2), UTI-bearing PLI mice. Error bars represent mean \pm S.E.M. **(L-M)** Flow cytometry analysis of mammary neutrophil populations from IgG treated (n=4) or anti-TIMP1 neutralizing antibody treated (n=2), UTI-bearing PLI mice. Error bars represent mean \pm S.E.M.